

For Reference

NOT TO BE TAKEN FROM THIS ROOM

Ex LIBRIS
UNIVERSITATIS
ALBERTAENSIS



THE UNIVERSITY OF ALBERTA

ELECTROCHEMISTRY OF THE GROUP IIIA AND GROUP IVA
ELEMENTS IN FUSED LiCl-KCl EUTECTIC

by



JOSEPH MEYER SHAFIR

A THESIS

SUBMITTED TO THE FACULTY OF GRADUATE STUDIES AND RESEARCH
IN PARTIAL FULFILMENT OF THE REQUIREMENTS FOR THE DEGREE


OF

DOCTOR OF PHILOSOPHY

DEPARTMENT OF CHEMISTRY

EDMONTON, ALBERTA

SPRING, 1973



Digitized by the Internet Archive
in 2024 with funding from
University of Alberta Library

<https://archive.org/details/Shafir1973>

ACKNOWLEDGEMENTS

I am most appreciative of the assistance and encouragement given to me by Dr. J. A. Flannery who so carefully supervised and guided this study since its inception.

Financial assistance from the National Science Council and the University of Alberta is gratefully acknowledged.

TO REL

A C K N O W L E D G E M E N T S

I am most appreciative of the assistance and encouragement given to me by Dr. J. A. Plambeck who so carefully supervised and guided this study since its inception.

Financial assistance from the National Research Council and the University of Alberta is gratefully acknowledged.

T A B L E O F C O N T E N T S

	<u>Page</u>
Acknowledgements	iii
Table of Contents	iv
List of Tables	vii
List of Figures	viii
<u>PART I:</u> Electrochemistry of the Group IIIA Elements in Fused LiCl-KCl Eutectic	
ABSTRACT	1
INTRODUCTION	2
Standard Potentials of The Group IIIA Elements	8
EXPERIMENTAL	12
Solvent	12
Apparatus	14
Chemicals	20
Procedure	21
RESULTS	24
Gallium	24
Indium	25
Thallium.	28
DISCUSSION	31
CONCLUSION	41
BIBLIOGRAPHY.	42

	<u>Page</u>
<u>PART II</u> : Electrochemistry of the Group IVA Elements in Fused LiCl-KCl Eutectic	
ABSTRACT	44
INTRODUCTION	46
Carbon	46
Silicon	46
Germanium	48
Tin.	56
Lead	57
EXPERIMENTAL	58
Apparatus	58
Procedure	63
Chemicals and Materials	67
RESULTS	68
Silicon	68
Germanium	73
Potentiometry	73
Voltammetry	77
Chronopotentiometry	78
Thermodynamics of Gold-	
Germanium Alloy Formation	86
Topography of Germanium Deposited onto Gold.	91
Tin.	101
Lead	106

	<u>Page</u>
Discussion of Standard Potentials	108
Stability of M(II) Oxidation State.	111
CONCLUSION	113
BIBLIOGRAPHY	114
APPENDIX I	118
Introduction	118
Literature	118
Experimental	119
RESULTS AND DISCUSSION	121
Manganese	121
Cobalt	121
Antimony	122
BIBLIOGRAPHY	125
APPENDIX II	126
POTENTIOMETRIC DATA	126
SAMPLE CALCULATION OF THE STANDARD POTENTIAL.	141

L I S T O F T A B L E S

<u>Table</u>		<u>Page</u>
<u>PART I</u>		
I	Standard Potentials of the Group IIIA Elements in LiCl-KCl Eutectic at 450°C	33
II	First Three Ionization Potentials of the Group IIIA Elements	35
III	M-Cl Bond Energies of the Group IIIA Elements	36
IV	Pauling Radii of the Group IIIA Elements	36
<u>PART II</u>		
I	Standard Potentials of Germanium Couples	77
II	Chronopotentiometric Data	84
III	Thermodynamics of Gold-Group IVA-Metal Alloys, 450°C	90
IV	Standard Potentials of the Group IVA Elements in LiCl-KCl Eutectic, 450°C	109
V	Stability of the M(II) Oxidation State of the Group IVA Elements in LiCl-KCl Eutectic at 450°C	111

L I S T O F F I G U R E S

<u>Figure</u>		<u>Page</u>
<u>PART I</u>		
1	Apparatus for Purifying LiCl-KCl Eutectic Melt	16
2	Electrochemical Cell	19
3	Typical Nernst Plot for the In(I)/In(0) Couple	26
4	Nernst plot for the Tl(III)/Tl(I) Couple	30
<u>PART II</u>		
1	Switching and Triggering Circuit for Chronopotentiometry of Germanium	61
2	Voltammetric Scans of Ge(II) in Fused LiCl-KCl Eutectic at 450°C, using a Tungsten Micro-electrode	79
3	Anodic Voltammogram of Electrodeposited Germanium on a Tungsten Microelectrode	80
4	Chronopotentiogram of 1.0×10^{-3} M Ge(II) taken in the Fused LiCl-KCl Eutectic at 450°C	82
5	Plot of Reciprocal Current versus $\tau^{\frac{1}{2}}$ for the First Transition in the Chronopotentiometric Analysis	83
6	Plot of Potential versus Temperature for the Cell Au-Ge(12 wt. % Ge, l)/Ge(II) in LiCl-KCl/Ge(s)	88
7	Anodic Chronopotentiogram of Germanium on a Gold Flag (0.4 cm ² in area)	92
8	Metallographs	99

PART IELECTROCHEMISTRY OF THE GROUP IIIA ELEMENTS INFUSED LiCl-KCl EUTECTICA B S T R A C T

Boron is electrochemically inactive in the fused LiCl-KCl eutectic. Reversible electrode potentials exist for aluminum, gallium, indium, and thallium in the LiCl-KCl eutectic melt at 450°C. The standard molar electrode potentials of the couples against a standard molar platinum electrode are: Al(III)/Al(0) : -1.762; Ga(III)/Ga(0) : -1.141 V; In(I)/In(0) : -1.215 V; In(III)/In(I) : -0.940 V; Tl(I)/Tl(0) : -1.465 V; Tl(III)/Tl(I) : +0.155 V. These oxidation states and potentials are discussed.

I N T R O D U C T I O N

The fused LiCl-KCl eutectic (59 mole percent LiCl, melting point 352°C) is one of the first fused salt systems in which detailed electrochemical studies have been undertaken. The first compilation of standard half-cell potentials in this melt was carried out by Laitinen and Liu (1). In determining half-cell potentials of various electrode systems, they made use of the Nernst equation in the form:

$$E = E^{\circ} - 2.303 \frac{RT}{nF} \log \frac{[\text{Red}]}{[\text{Ox}]}, \text{ where}$$

E = the observed potential of the electrode being studied;

E° = the standard potential of the experimental half-cell;

R = the gas constant ($8.31470 \text{ J deg}^{-1} \text{ mole}^{-1}$);

T = the temperature in degrees Kelvin;

n = the number of electrons transferred;

F = the Faraday constant ($96,493.5 \text{ J V}^{-1} \text{ equivalent}^{-1}$);

$[\text{Red}]$ = the reductant concentration;

$[\text{Ox}]$ = the oxidant concentration.

The operating temperature for work in the fused LiCl-KCl eutectic has been standardized by Laitinen and Liu (1), and others following them, at 450°C. At this temperature, the value of $2.303 RT/nF$ for a one-electron process is

0.1434 volts.

It should be noted that the Nernst equation given does not include terms for the activity coefficients of the reductant or oxidant. These are not included, as it is most often found that, for the concentration ranges of metal ions employed, plots of E versus $\log[\text{Red}]/[\text{Ox}]$ are linear. This means that the activity coefficients of the reduced and oxidized species are constant - more generally that their ratio is constant - and the activity coefficients may be separated from the concentration terms and incorporated as part of the E° value. Thus, while the complete Nernst equation is given by

$$E = E^\circ' - 2.303 \frac{RT}{nF} \log \frac{\gamma_{\text{Red}}[\text{Red}]}{\gamma_{\text{Ox}}[\text{Ox}]},$$

where E°' is the thermodynamic standard potential and γ is the activity coefficient, this equation can be expanded to:

$$E = E^\circ' - 2.303 \frac{RT}{nF} \log \frac{[\text{Red}]}{[\text{Ox}]} - 2.303 \frac{RT}{nF} \log \frac{\gamma_{\text{Red}}}{\gamma_{\text{Ox}}}.$$

As long as the ratio of the activity coefficients remains constant, the latter equation may be reduced to the equation presented on page 2, i.e., by adding E°' and $-2.303 \frac{RT}{nF} \log \gamma_{\text{Red}}/\gamma_{\text{Ox}}$ to give E° , the observed standard potential. (In dealing with a metal/metal ion couple, the activity of the pure metal is taken as unity, and then one is only concerned with the constancy of the activity coefficient of the metal ion since the metal is present in

the pure state).

Definition of standard states is required before a compilation of standard electrode potentials can be made in any solvent system. Since the standard operating temperature for work done in the fused LiCl-KCl eutectic is 450°C, the standard state of metals in the melt is taken as their actual physical state at this temperature and at one atmosphere pressure, and their activity under these conditions is defined to be unity. The standard state of a metal ion is taken as unit concentration, with the activity coefficient of the metal ion at unit concentration taken to be that of the ion in an infinitely dilute solution. The standard state of gases is taken as the pure gas at one atmosphere pressure (and at 450°C). The standard potential of a redox couple is obtained by solving for E° in the Nernst equation once the concentration-potential data are known. A special case exists for solutions where both the reductant and oxidant concentrations are independent of one another, such as the Fe(III)/Fe(II) couple. In this type of system, when solutions at different concentrations of oxidant or reductant are prepared, the observed potential is equal to the standard potential whenever the term $\log[\text{Red}]/[\text{Ox}]$ in the Nernst equation equals zero.

Three electromotive force series in a given solvent may be set up depending upon which concentration scale is

used to express the concentrations of the oxidant and reductant: molar(\underline{M}), molal(m), and mole fraction (X). Because the definition of the standard state for all ions is unit concentration, and the behavior of the ion at unit concentration is taken to be that of the ion in an infinitely dilute solution, the molar and molal concentration scales are more convenient to use in expressing solute concentrations, since at unit concentration on the molar and molal scales there exists a relatively dilute solution of the ion. The mole fraction concentration scale is also used to set up an electromotive force series, but its use is not as reasonable as the use of the molar and molal scales, because unit mole fraction - the standard state of the solute on this scale - corresponds to the pure compound, and the behavior of the solute at unit mole fraction is taken as if the solute were in an infinitely dilute solution. The concept of the concentration of a solution can be defined to be an amount of solute dissolved in a quantity of solvent. At unit mole fraction of solute, no solvent is present, and hence no solution, as defined, exists. Thus the previous phrase "the behavior of the solute at unit mole fraction is taken as if the solute were in an infinitely dilute solution" does not correspond to a physically meaningful situation. When the solvent density is unknown, the electromotive force series is usually based upon the molal concentration scale. Due to experimental difficulty in the measurement of volume at high

temperatures, the molar concentration scale can be used to express reductant or oxidant concentrations only when the density of the solvent is known. The density of the fused LiCl-KCl eutectic was determined by Van Artsdalen and Yaffe (2), and its value at 450°C is 1.648 gm/ml. The relationship between molality and molarity, and mole fraction and molarity was calculated by Laitinen and Liu (1) for the fused LiCl-KCl eutectic at 450°C to be $m = 0.607 \text{ M}$ and $X = 0.0337 \text{ M}$.

The half-cell potentials in any electromotive force series are listed with respect to a reference electrode whose standard potential is arbitrarily (and conveniently) set to zero. In the fused LiCl-KCl eutectic, the most commonly used reference electrode has been the Pt(II)/Pt(0) couple. The Ag(I)/Ag(0) and chlorine gas/chloride ion couples have also been used as reference electrodes. The Pt(II)/Pt(0) reference electrode is generated by electrolytic anodization of platinum metal. It has been shown by Asakura and Mukaibo (3) that the use of large current densities to generate Pt(II) results in passivation of the platinum metal electrode with a layer of K_2PtCl_6 . As a result, low current densities must be employed for the electrolytic generation of Pt(II). (De Haan and Vander Poorten (4), Pointud, Hladik, and Morand (5), and Laitinen, Tischer, and Roe (6) have also reported the anodic passivation of platinum). Low concentrations of Pt(II) (con-

centrations in the range of 0.01 to 0.1 M are practical; the upper concentration limit is not precisely known) must also be used, because it was shown by De Haan and Vander Poorten (4) that at higher concentrations the equilibrium disproportionation of Pt(II) takes place: $2\text{Pt(II)} \rightleftharpoons \text{Pt(0)} + \text{Pt(IV)}$. Asakura and Mukaibo (7) have shown that coulometric anodization of silver, even at large current densities, leads to no passivation of the metal, and silver is therefore preferred by some workers over platinum as a reference electrode. A disadvantage does exist with the Ag(I)/Ag(0) reference electrode, and that is the extensive recrystallization of silver from the metal into the melt. This phenomenon, however, does not appear to affect the potential of the Ag(I)/Ag(0) couple. The standard potential of the Ag(I)/Ag(0) couple was determined by Laitinen and Liu (1) and has a value of -0.743 ± 0.002 V (with respect to the standard molar platinum electrode [s.m.p.e.]). Use of the chlorine reference electrode, where chlorine is bubbled over graphite, is possible but inconvenient. The standard potential of the chlorine gas/chloride ion electrode has been determined by Laitinen and Pankey (8) to be $+0.322 \pm 0.002$ V (versus the s.m.p.e.).

All potentiationmetric work presented in this thesis employed the Pt(II)/Pt(0) couple as the reference electrode. The reversibility of this electrode has been established by Laitinen and Liu (1). Passivation of the

platinum electrode was never observed by the present author either during the generation of Pt(II) or after the Pt(II)/Pt(0) reference system had been established. The polarization potential of the cell Pt/Pt(II), LiCl-KCl//LiCl-KCl/Li/C during the generation of Pt(II) (and simultaneous deposition of lithium onto a graphite cathode) never exceeded the potential of lithium deposition (-3.3 V). This means that passivation of the platinum electrode did not take place since formation of passivating - and electrically insulating - layer of K_2PtCl_6 on the platinum electrode would impede current passage through the above cell and a polarization potential greatly exceeding 3.3 V would have been observed. Low concentrations, approximately 0.005 to 0.01 M of Pt(II), were employed to ensure that disproportionation of Pt(II) would not occur. Once the Pt(II)/Pt(0) reference electrode was prepared, the platinum surface always remained bright, showing the absence of film formation (K_2PtCl_6 or deposition of platinum metal from the disproportionation of Pt(II)). Thus the Pt(II)/Pt(0) redox couple served as a functional reference electrode.

Unless otherwise stated, all potentials in this thesis are reported on the molar concentration scale with respect to the s.m.p.e.

Standard Potentials of the Group IIIA Elements

No reversible potentials of boron couples in this

melt are known. Plambeck and Chapman (9) found that boron does not react with the melt, and attempts by them to coulometrically anodize boron only resulted in chlorine evolution; thus further study of this element in the eutectic melt was abandoned.

The standard potential of the Al(III)/Al(0) couple has been determined by Laitinen and Liu (1) to be -1.762 ± 0.009 V. Since aluminum chloride - at high concentrations - is volatile from the eutectic melt, two procedures were employed to obtain concentration-potential data. For low concentrations of aluminum chloride, where volatilization was not severe, small amounts of the compound were added to the melt, and the potential of the resulting solution was determined with an aluminum wire. Attainment of higher aluminum chloride concentrations involved coulometric anodization of an aluminum wire. After the equilibrium rest potential had been recorded, the aluminum compartment was immediately removed from the bulk melt and its contents were analyzed for aluminum.

Gallium and indium metals are both liquid at 450°C , and they do not react with the melt at this temperature. Their standard potentials were originally determined in the fused LiCl-KCl eutectic by Laitinen and Liu (1) who added a weighed amount of the anhydrous MCl_3 salt to the eutectic and coulometrically deposited some of the metal onto a tungsten microelectrode which then served as the

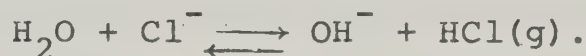
indicator electrode. Further potential readings were obtained by successive reductions of the metal chlorides. In this manner, the following standard potentials were reported: Ga(III)/Ga(0) , -0.84 ± 0.02 V and In(III)/In(0) , -0.800 ± 0.009 V. Their potential- $\log[\text{Ga(III)}]$ plot had a slope close to a one-electron transfer, rather than a three-electron transfer. It was stated by Laitinen and Liu (1) that serious difficulties were experienced in transferring gallium trichloride to the eutectic, since the salt is extremely deliquescent. As a result, formation of complex species of gallium(III) would set up a mixed potential system and probably lead to an incorrect value for the Ga(III)/Ga(0) standard potential. Anders and Plambeck (10) carried out an electrochemical study of various elements in a fused tetrachloroaluminate melt and have shown the monovalent oxidation states of gallium and indium to be of importance in that medium, and a Raman study by Clarke and Hester (11) has shown the existence of In(I) in the fused LiCl-KCl eutectic. As a result, the oxidation states and standard potentials of indium and gallium were reinvestigated in the fused LiCl-KCl eutectic by the present author.

Thallium metal is liquid at 450°C , and does not react with the melt. Its standard potential was determined by Laitinen and Liu (1) in the same manner as described for gallium and indium. The standard potential of the

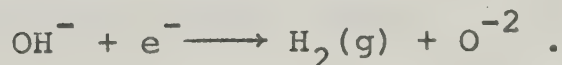
Tl(I)/Tl(0) couple was determined to be -1.476 ± 0.002 V. Delarue (12), in a voltammetric study of thallium in the fused LiCl-KCl eutectic, has reported the oxidation of Tl(I) to Tl(III) at a graphite electrode. The half-wave potential for this process was given as +0.2 V. This value is in agreement with the standard potential of +0.155 V for the Tl(III)/Tl(I) redox couple which was determined by the present author.

E X P E R I M E N T A LSolvent

The solvent used was the fused eutectic mixture of lithium chloride and potassium chloride. Purification of this melt is necessary before it can be used as a solvent in which electrochemical studies are to be undertaken. Water is the major impurity, and is absorbed by lithium chloride which is highly deliquescent. Fusion of the salts results in the reaction:



The hydroxide so produced attacks the container material (Pyrex glass) and interacts with the electroactive ions of interest to form oxy-species. Moreover, the hydroxide ion limits the cathodic potential range of the melt to about -1 V, since reduction of hydroxide takes place at this potential:

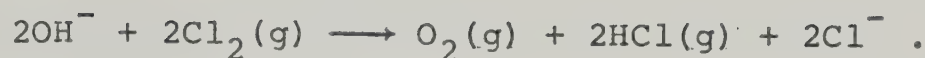


Thus, removal of water and hydroxide is imperative, and several methods have been employed to accomplish this. Laitinen, Ferguson, and Osteryoung (13) dried the salt mixture at room temperature for three days under vacuum, and then raised the temperature of the salt mixture to 300°C over an eight hour period. Hydrogen chloride gas

was introduced into the salt mixture - to reverse the above hydrolytic reaction and drive off the water so formed - and was allowed to flow as the mixture was fused and raised to 500°C. The excess hydrogen chloride was removed using a water aspirator, followed by evacuation on a vacuum manifold. Removal of heavy metal impurities from the melt can be implemented by their simple displacement using a more electroactive metal like magnesium, as was proposed by Laitinen, Tischer, and Roe (6). Since the standard potential of magnesium is very negative, -2.580 V (1), negligible interference between Mg(II) and the system to be studied in the melt should be encountered as long as the standard potential of the system to be studied is more positive than that of the Mg(II)/Mg(0) couple. Inman, Hills, Young, and Bockris (14) employed a purification procedure which involved use of the hydrogen chloride gas treatment followed by electrolytic removal of other impurities (under vacuum) using tungsten or molybdenum cathodes and carbon anodes.

For the experimental work reported in this thesis, the LiCl-KCl eutectic melt was purified according to the procedure of Maricle and Hume (15) in conjunction with the magnesium treatment of Laitinen, Tischer, and Roe (6). The method involves flushing the fused eutectic (at 450°C) with a stream of chlorine gas; the hydrolytic products formed upon salt fusion are removed according to the

reaction:



Maricle and Hume (15) found that a forty minute chlorine treatment followed by a twenty minute argon flush (to remove excess chlorine) was sufficient to remove all water from the melt. In addition to this, polished magnesium ribbon was introduced into the melt (argon bubbling being maintained) for a period of fifteen minutes. Voltammetric scans of the melt thus prepared, using a graphite indicating electrode, exhibited a very low residual current (1 microampere at an electrode 0.05 cm^2 in area), and did not indicate the presence of hydroxide. Further evidence of the purity of the melt was exhibited in the observation that the melt did not attack its Pyrex glass container even after five days of contact with it. Thus, the method used in purifying the eutectic melt is extremely convenient as the time required to carry out the procedure is short when compared to the time required by the other available methods.

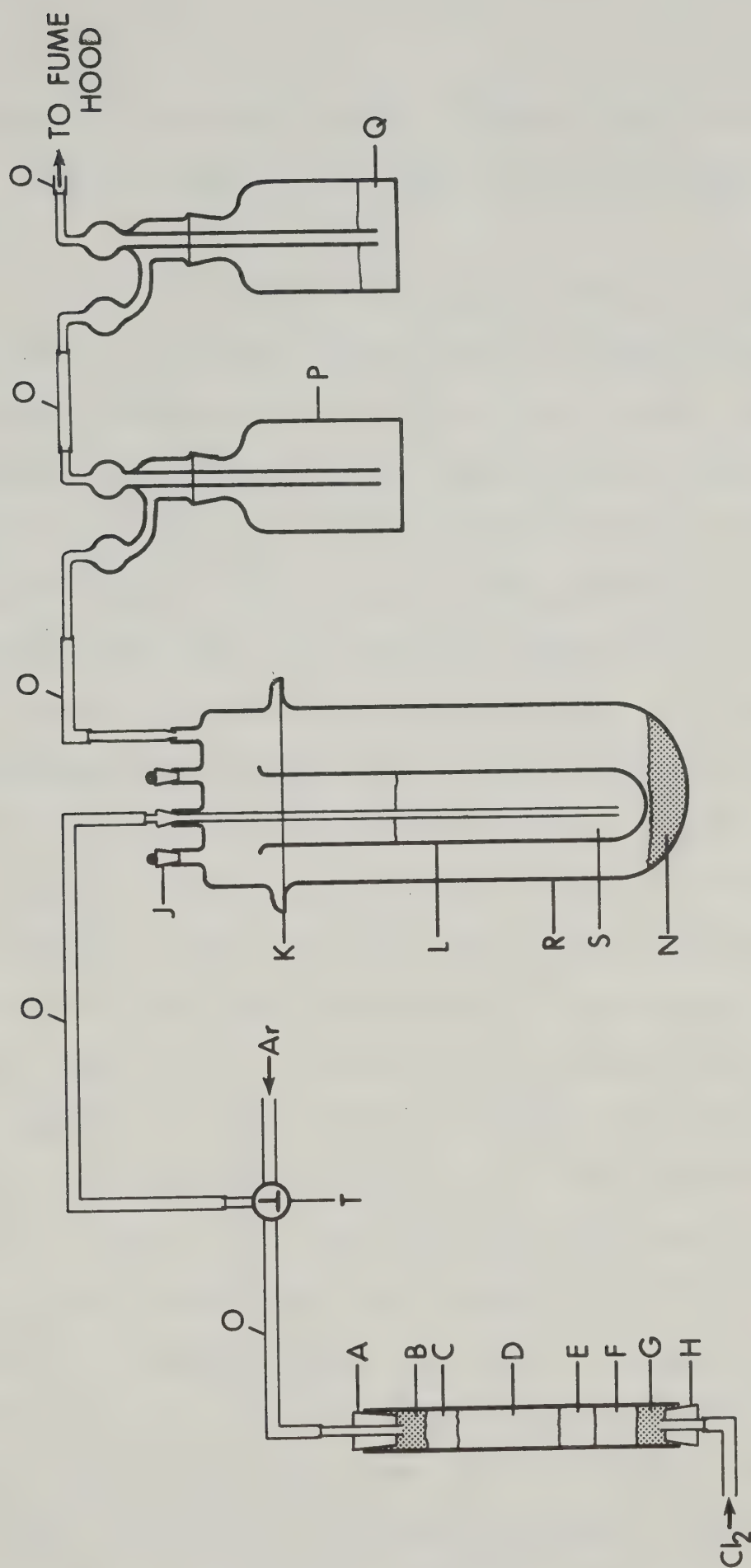
Apparatus

The apparatus used in the melt preparation is shown in Figure 1. Once prepared, the eutectic was stored under an argon atmosphere by clamping the outside Pyrex tube and cell head together, and allowing the apparatus to cool.

FIGURE 1

Apparatus for Purifying LiCl-KCl Eutectic Melt

A,H.	Teflon taped rubber stoppers.
B,G.	Glass wool.
C,E.	Drierite - indicating.
F.	Adsorption charcoal.
D.	Drierite - ordinary.
J.	Standard taper 14/20 glass stopper.
K.	O ring.
L.	Pyrex tube.
R.	Outer Pyrex container.
S.	Fused LiCl-KCl eutectic.
N.	Glass wool.
O.	Teflon tubing.
P.	Gas wash bottle.
Q.	Concentrated sulfuric acid (to monitor gas flow).
T.	T-joint stop-cock.



The eutectic produced in this manner could be stored for very long periods of time (six months or more) before being used.

The electrochemical cell, as shown in Figure 2, consisted of an outer Pyrex container which housed a Pyrex crucible containing about 120 cm^3 of eutectic at 450°C . Isolation compartments were constructed by extending 10 mm Pyrex tubes that were sealed at one end by a D porosity sintered glass disk (Ace Glass Co., Vineland, N.J.). The platinum reference electrode was composed of a platinum flag pressure-welded to a platinum wire, the platinum wire being housed in a Pyrex tube. The counter electrode was made of graphite (spectroscopic electrode SPK, 0.120" diameter x 12" long, Union Carbide Corp., New York), and was suspended into the melt from a piece of copper tubing, the top of which was sealed onto a copper wire that led out of the cell. A chromel-alumel thermocouple sheathed in a Pyrex tube and calibrated against the melting point of zinc was used to monitor the solution temperature. The gallium, indium, and thallium electrodes were designed as cups, since these metals are liquid at 450°C . They consisted of a uranium glass tube with a tungsten wire protruding from it. A small uranium glass cup was attached to the end of the tube such that the tungsten lead extended into the cup and was completely covered by the molten metal after the cup was filled with the solid metal and placed

FIGURE 2

Electrochemical Cell

- A. Cell head. Bottom flange is a 76/50 ball joint mounted on an O ring, B.
- C. Isolation compartment; M. Extra isolation compartment.
- D. Copper tubing to support graphite counter electrode, E.
- F. Indicating electrode.
- G. Outer Pyrex container.
- H. Pyrex crucible.
- I. Platinum reference electrode.
- J. Argon gas inlet.
- K. Cork stopper with a wedge cut: (a) to allow space for the copper wire coming from the copper tubing and, (b) to act as a vent for the release of excess argon.
- L. Pyrex tube, housing the chromel-alumel thermocouple.
- N. Eutectic melt level.
- O. Liquid metal pool.
- P. Glass wool.

14/20

A

B

C

D

E

F

G

H

I

K

L

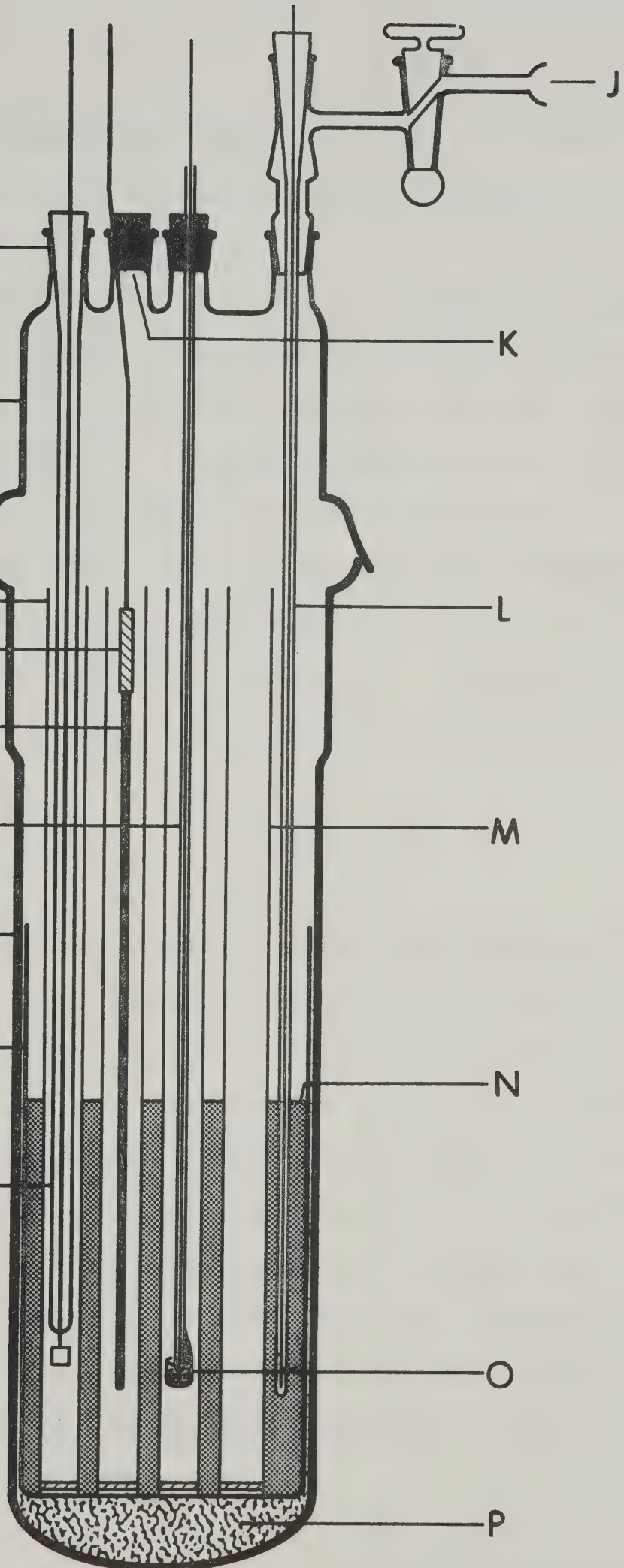
M

N

O

P

J



into the electrochemical cell. The effect of this was to provide a metal pool electrode 7 mm in diameter for coulometric anodizations.

The cell was heated to 450°C by means of a Lindberg Hevi-Duty 54331-A oven (Sola Basic Industries, Watertown, Wisc.) mounted in the vertical position, and this temperature was maintained by a Lindberg Hevi-Duty 59344 temperature controller. Potentials were measured with a Hewlett-Packard Model 3400A digital voltmeter equipped with a Hewlett-Packard 3444A DC multifunctional unit. A Model IV coulometric Current Source (E. H. Sargent and Co., Chicago) was used for the anodization of the metals into solution.

Chemicals

Reagent grade lithium chloride and potassium chloride as well as the magnesium ribbon used in the melt purification were obtained from Fisher Scientific. Platinum wire and foil used in the construction of the reference electrode were obtained from Engelhard Industries of Canada. Gallium, 99.99% pure, was obtained from A. D. Mackay Inc., New York, and indium (electronic material, 99.999% pure) from Cominco Ltd., Montreal: both metals were in wire form. Thallium, in shot form, was 99.9999% pure, and was obtained from Alfa Inorganics Beverly, Massachusetts.

Procedure

All glassware which came into contact with the eutectic melt was cleaned by being boiled in perchloric acid. The glassware was then dried and stored at 110°C until used. (Graphite electrodes were also dried at 110°C prior to use). The purified eutectic was fused under an atmosphere of argon, after which the fritted (isolation) compartments were placed into the melt. These compartments not only isolated the anolyte, catholyte, and reference electrode solutions, but also filtered the melt as it rose into the compartments. Vacuum was then applied to the system to remove any air that may have entered when the isolation compartments were placed into the melt. Argon was then introduced to blanket the cell. Experimental work commenced after the electrodes had been placed in their respective compartments and the melt level in the compartments was equal to that of the bulk melt.

Thallium readily oxidizes in air, and the shot metal obtained from the manufacturer was coated with a brown-black layer of Tl_2O . Since Tl_2O is soluble in the fused LiCl-KCl eutectic (12), the metal pool was allowed to remain in contact with the bulk melt for a period of about 18 hours before being transferred to an isolation compartment. This resulted in the dissolution of the Tl_2O and the production of a bright pool of liquid thallium.

Anodization of the gallium, indium, and thallium pools resulted in the formation of Ga(III) , In(I) , and Tl(I) , respectively. After the removal of the indium and thallium metal pools, In(I) and Tl(I) were further oxidized to the M(III) oxidation state at a graphite rod identical to the one being used as the counter electrode, as shown in Figure 2.

The thermoelectric potential between graphite and platinum, and tungsten and platinum, was determined at 450°C by short circuiting the hot ends of a platinum wire and graphite electrode, and a platinum wire and a tungsten lead, respectively. The graphite electrode was found to be 0.004 V positive with respect to platinum, and the tungsten electrode was found to be 0.005 V positive with respect to platinum. These thermoelectric potentials were appropriately subtracted from the experimentally determined standard potential.

Calculation of the gallium and indium standard electrode potentials was carried out on the University of Alberta IBM System/360 computer (16). All potentials are reported with respect to the appropriate standard platinum electrode on the molar, molal, and mole fraction scales. Volumes of the isolation compartments were determined by argentometric titration of their chloride contents. This information, in conjunction with the amount of current used to anodize the liquid metal pool, allowed the calcu-

lation of solute concentrations.

R E S U L T SGallium

In the determination of the Ga(III)/Ga(0) standard potential, a total of twenty-seven concentration-potential data points were taken in three separate coulometric anodizations of the gallium pool electrode. The current density employed for these anodizations was 20 mA/cm^2 , and the concentration of Ga(III) was varied over the range from 2.33×10^{-3} to $6.86 \times 10^{-2} \text{ M}$. Higher concentrations were not attempted because at concentrations of Ga(III) greater than about 0.07 M , volatilization of GaCl_3 became noticeable. A plot of the cell potential (corrected to the s.m.p.e.) as a function of the logarithm of the Ga(III) concentration was linear, and had a slope of $0.061 \pm 0.006 \text{ V/log unit}$. This value is in fair agreement with the theoretical value of 0.048 V/log unit expected for a three-electron process at the operating temperature employed. The standard potential of the Ga(III)/Ga(0) redox couple was determined from the intercept of the plot, corrected for the thermoelectric potential of 0.005 V between platinum and tungsten, and was found to be $-1.141 \pm 0.008 \text{ V}$. Any attempts to further oxidize the Ga(III) produced, using a graphite rod, resulted in immediate chlorine evolution. This shows that stable lower (e.g. Ga(I)) or higher oxidation states of gallium do not exist in the melt.

Indium

A total of thirty-five concentration-potential data points were taken in four separate coulometric anodizations of the indium pool electrode. The current density employed in these anodizations was 20 mA/cm^2 , and the concentration of In(I) ranged from 8.74×10^{-3} to 0.340 M . A plot of the cell potential (corrected to the s.m.p.e.) as a function of the logarithm of In(I) concentration was linear, and had a slope of $0.138 \pm 0.010 \text{ V/log unit}$, in agreement with the theoretical value of 0.143 V/log unit for a one-electron process at 450°C . The standard potential of the $\text{In(I)}/\text{In(0)}$ redox couple was determined from the intercept of the plot, corrected for the thermoelectric potential between platinum and tungsten, and was found to be $-1.215 \pm 0.012 \text{ V}$. A typical Nernst plot for the $\text{In(I)}/\text{In(0)}$ redox couple is shown in Figure 3.

During the oxidation of indium metal, a small amount of yellow-red material, most probably InCl , condensed in the upper, cool part of the isolation compartment. The volatilization of InCl was unavoidable and led to a decreased concentration of In(I) in solution. This effect would lead to a value of the standard potential which may be too positive. However, as the amount of InCl which volatilized from solution appeared to be quite small, this effect is estimated to be not more than 5 mV .

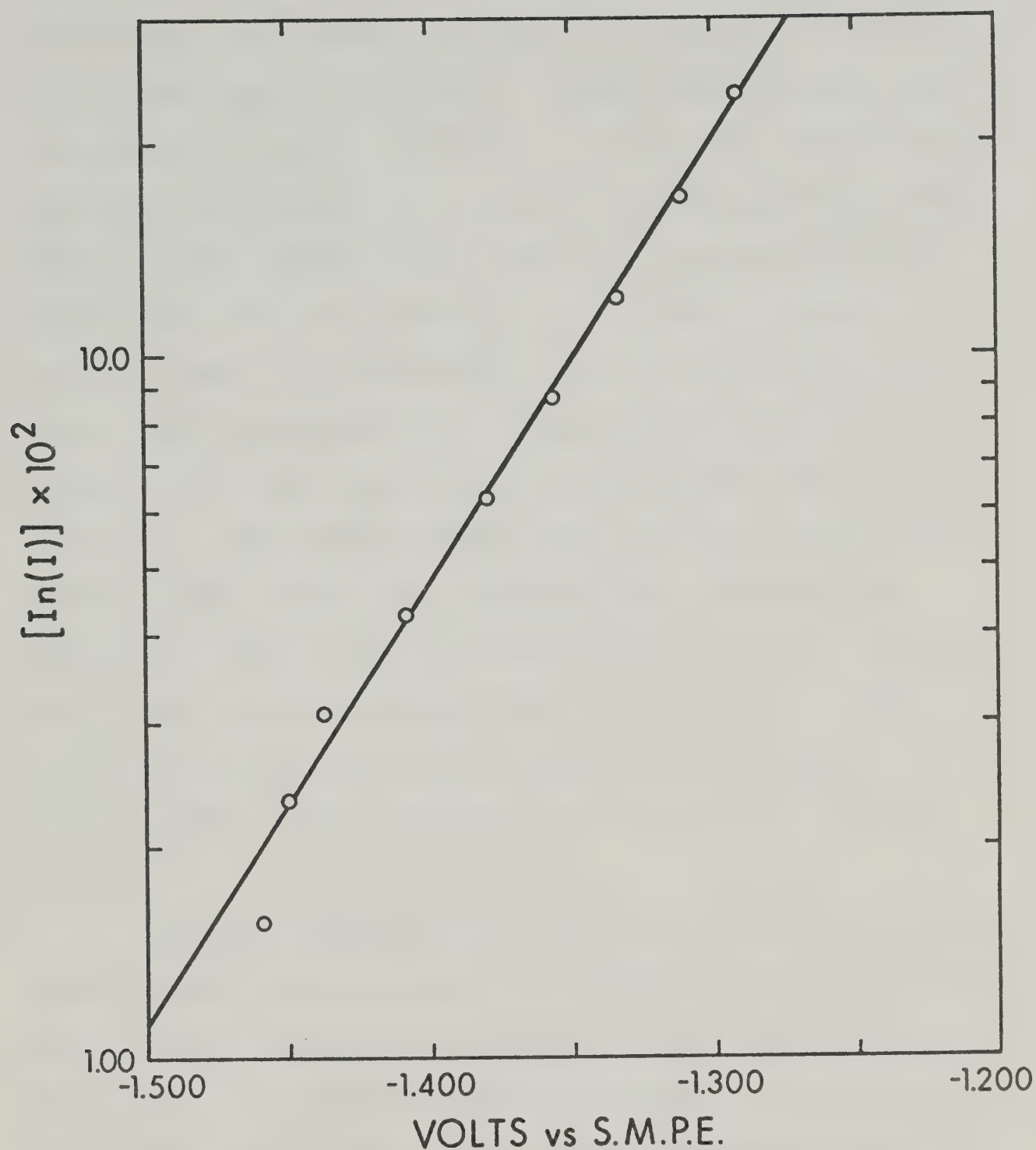


Figure 3. Typical Nernst plot for the In(I)/In(0) couple. In(I) concentration is in units of molarity. No correction for the thermoelectric potential between platinum and tungsten is shown.

Solutions of In(I), produced by anodization of indium metal, were further oxidized at a graphite electrode. The current density employed in these oxidations was approximately 1 mA/cm^2 . A total of twenty-two concentration-potential data points were taken in three separate experiments, and the concentration ratio of In(I)/In(III) was varied over the range from 151.0 to 0.4133. A plot of the cell potential (corrected to the s.m.p.e.) as a function of the logarithm of the concentration ratio of In(I)/In(III) was linear and had a slope of $0.076 \pm 0.004 \text{ V/log unit}$. This value agrees well with the theoretical value of 0.072 V/log unit expected for a two-electron process at 450°C . The standard potential of the In(III)/In(I) redox couple obtained from the intercept of the plot, and corrected for the thermoelectric potential between platinum and graphite, was found to be $-0.940 \pm 0.005 \text{ V}$.

From the standard potentials of the In(I)/In(0) and In(III)/In(I) redox couples, the standard potential of the In(III)/In(0) couple was calculated to be $-1.032 \pm 0.013 \text{ V}$. These data (i.e., the standard potentials of In(I)/In(0) and In(III)/In(I)) also allow the equilibrium constant, K , for the reaction $3\text{In(I)} \rightleftharpoons 2\text{In(0)} + \text{In(III)}$ to be calculated. The value of $K = [\text{In(III)}]/[\text{In(I)}]^3$ is $1.46 \times 10^{-4} \text{ l}^2 \text{ mol}^{-2}$.

Thallium

For the determination of the standard electrode potential of the $\text{Tl(III)}/\text{Tl(I)}$ redox couple, a solution of Tl(I) was generated by coulometrically oxidizing a liquid thallium pool. In the course of this generation, ten concentration-potential data points were collected in order to determine the value of the $\text{Tl(I)}/\text{Tl(0)}$ standard potential, and then compare it with the value obtained by Laitinen and Liu (1) who electrolytically reduced Tl(I) (added to the melt as anhydrous thallium (I) chloride) at a tungsten electrode. The current density employed in the anodization of the thallium pool was 20 mA/cm^2 , and the concentration range of Tl(I) over which data was collected was 2.08×10^{-2} to 0.148 M . A plot of the cell potential against the logarithm of Tl(I) concentration was linear and had a slope of $0.140 \pm 0.002 \text{ V/log unit}$, in agreement with the theoretical value of 0.143 V/log unit for a one-electron process at 450°C . The standard potential of the $\text{Tl(I)}/\text{Tl(0)}$ redox couple was calculated to be $-1.465 \pm 0.002 \text{ V}$. This value, corrected for the thermoelectric potential between platinum and tungsten, compares favourably to the value of $-1.476 \pm 0.002 \text{ V}$ determined by Laitinen and Liu (1).

Thallium (I), produced by the coulometric oxidation of elemental thallium, was further oxidized at a graphite

electrode. The current density employed in this process was 0.6 mA/cm^2 . A total of thirty concentration-potential data points was taken in two separate experiments in which the concentration ratio of $\text{Tl(I)}/\text{Tl(III)}$ ranged from 27.57 to 1.222. The solution of Tl(I) was colorless, but turned light green when Tl(III) was generated. A plot of the cell potential as a function of $\log [\text{Tl(I)}]/[\text{Tl(III)}]$ was linear (Figure 4), and had a slope of 0.074 ± 0.002 V/log unit. This value is in agreement with the theoretical value of 0.072 V/log unit for a two-electron process at 450°C . The standard potential of the $\text{Tl(III)}/\text{Tl(I)}$ redox couple was calculated to be $+0.155 \pm 0.002$ V. This value has been corrected for the thermoelectric potential between graphite and platinum.

From the standard potentials of the $\text{Tl(I)}/\text{Tl(0)}$ and $\text{Tl(III)}/\text{Tl(I)}$ redox couples, the standard potential of the $\text{Tl(III)}/\text{Tl(0)}$ redox couple was calculated to be -0.385 ± 0.003 V, and the equilibrium constant for the reaction $3\text{Tl(I)} \rightleftharpoons \text{Tl(III)} + 2\text{Tl(0)}$ was calculated to be $2.55 \times 10^{-23} \text{ l}^2 \text{ mol}^{-2}$. Thus, thallium metal will quantitatively react with Tl(III) to produce Tl(I) .

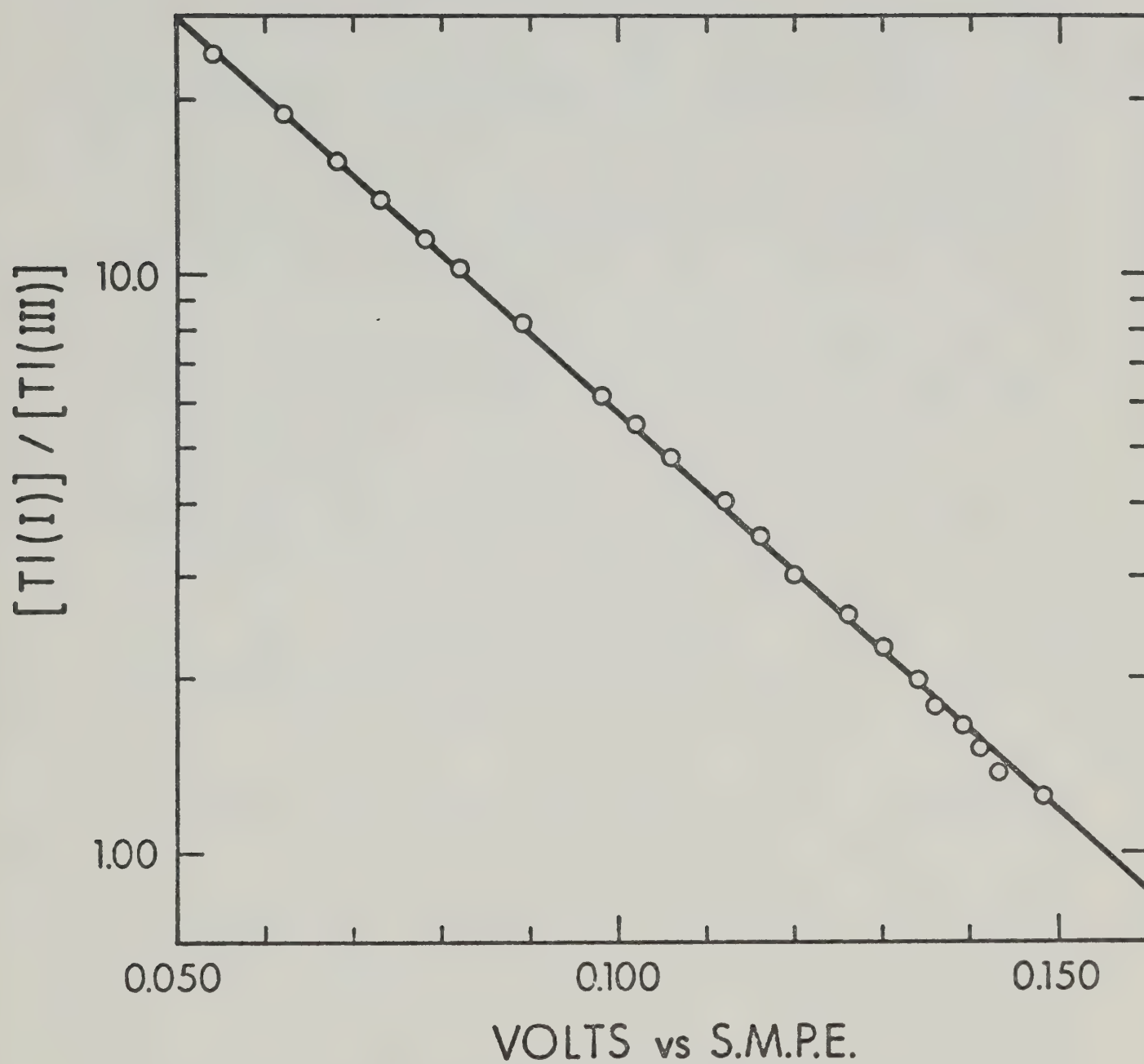


Figure 4. Nernst plot for the Tl(III)/Tl(I) couple. Potential is corrected for the thermoelectric potential of 0.004 V between graphite and platinum.

D I S C U S S I O N

Studies of gallium by McMullen and Corbett ((17), and references cited therein) and indium by Clark, Griswold, and Kleinberg ((18), and references cited therein) have shown that stable compounds of Ga(I) and In(I) do exist; the "divalent" state of these elements is really a I-III compound. A study by Anders and Plambeck (10) in a fused tetrachloroaluminate melt has shown the existence of In(I) and Ga(I), and the standard potentials of the Ga(I)/Ga(0), Ga(III)/Ga(0), and In(III)/In(I) couples were determined in that medium. In the study by Laitinen and Liu (1) of indium and gallium, the standard electrode potentials reported for the Ga(III)/Ga(0) and In(III)/In(0) couples (-0.84 ± 0.02 V and -0.800 ± 0.009 V, respectively) were obtained by adding the respective metal trichloride to the melt and carrying out a coulometric reduction. It was assumed that the reduction took place in one stage, viz., to the metal. In the present study, in which the metal was coulometrically anodized, oxidation to the tri-valent state was observed only for gallium. Thus, the assumption made by Laitinen and Liu (1) that gallium trichloride is reduced directly to the metal, was correct. Indium, however, was anodized first to the monovalent state, the stability of which has been confirmed in the fused LiCl-KCl eutectic by the Raman study of Clarke and Hester (11), and could not be further oxidized in the

presence of metallic indium. It is therefore concluded that the previously measured indium potential (1) corresponded to the In(III)/In(I) couple rather than the reported In(III)/In(0) couple. The data presented in reference 1 appear to be insufficient to distinguish the exact oxidation state to which reduction actually occurred.

It is not surprising that the standard electrode potentials of gallium and indium determined in this study are significantly different from those observed in the previous work (1), since the trichlorides of gallium and indium are somewhat volatile at these temperatures. The direct addition procedure of Laitinen and Liu (1) would lead to considerably greater loss of the trichloride than the electrochemical generation procedure employed in the present work, and hence to considerably more positive standard potential values. Also, since Ga(III) was generated in the eutectic melt and not added as the trichloride (which is highly deliquescent), the problem of aqueous contamination of the system was significantly reduced. It is felt that for these reasons, and because considerably more data were obtained in this study, the values of the standard potentials of gallium and indium presented in this study are to be preferred.

A summary of the standard electrode potentials of the group IIIA elements on the molar, molal, and mole fraction scales is presented in Table I. Proceeding from

TABLE IStandard Potentials of the Group IIIA Elements inLiCl-KCl Eutectic at 450°C

<u>System</u>	<u>E°_{molar}</u>	<u>E°_{molal}</u>	<u>E°_x</u>	<u>Standard Deviation</u>
B	>+0.322	>+0.306	>+0.216	-
Al(III)/Al(0) [†]	-1.762	-1.767	-1.797	0.009
Ga(III)/Ga(0)	-1.141	-1.146	-1.176	0.008
In(III)/In(0)*	-1.032	-1.037	-1.067	0.013
Tl(III)/Tl(0)*	-0.385	-0.390	-0.420	0.003
In(III)/In(I)	-0.940	-0.956	-1.046	0.005
Tl(III)/Tl(I)	+0.155	+0.139	+0.049	0.002
Al(I)/Al(0)	>-1.762	>-1.767	>-1.797	-
Ga(I)/Ga(0)	>-1.141	>-1.146	>-1.176	-
In(I)/In(0)	-1.215	-1.199	-1.109	0.012
Tl(I)/Tl(0)	-1.465	-1.449	-1.359	0.002
Tl(I)/Tl(0) [†]	-1.476	-1.460	-1.370	0.002

[†] Reference 1.

* Calculated from experimental free energies.

aluminum to thallium, it is observed that the potentials of the $M(\text{III})/M(0)$ and $M(\text{III})/M(\text{I})$ couples increase while the potentials of the $M(\text{I})/M(0)$ ($M = \text{In}$ and Tl) couples decrease. This behavior can, in part, be explained on the basis of the ionization potentials of the group IIIA elements, and the strength of the $M\text{-Cl}$ bond formed in the complex ions of these metals. These values are summarized in Tables II and III respectively. It should be noted that the $M\text{-Cl}$ bond energies given in Table III apply only to the gaseous diatomic molecules, and not to the $M\text{-Cl}$ bond of the complex ion in solution. However, as a first approximation, it may be postulated that the order of bond strengths between the metal ion and chloride ion of the complex in the fused LiCl-KCl eutectic is: $(\text{B-Cl}) > \text{Al-Cl} > \text{Ga-Cl} > \text{In-Cl} > \text{Tl-Cl}$. If it is assumed that complexes of the type MCl_4^- and MCl_4^{-3} are formed for the $M(\text{III})$ and $M(\text{I})$ oxidation states respectively, then the order of the postulated $M\text{-Cl}$ bond strengths can be rationalized on the basis of an electrostatic model: in going down the group (boron to thallium), the size of the $M(\text{I})$ and $M(\text{III})$ ions increase (Table IV), and hence the charge density on the respective group IIIA metal ion decreases. As a result, the attractive force between the metal ion and the chloride ion will decrease, which is to say that weaker $M\text{-Cl}$ bonds are formed in going from boron to thallium.

TABLE II

First Three Ionization Potentials of the Group IIIA Elements (19)

Element	Ionization Potential (e.v.)			$\sum(I + II + III)$	$M(0) \rightarrow M(III) + 3e^-$	$\sum(II + III)$	$M(I) \rightarrow M(III) + 2e^-$
	I	II	III				
B	8.289	25.154	37.930	71.373		63.084	
Al	5.986	18.828	28.447	53.261		47.275	
Ga	5.999	20.51	30.71	57.22		51.22	
In	5.786	18.869	28.03	52.69		46.90	
Tl	6.108	20.428	29.83	56.37		50.26	

TABLE IIIM-Cl Bond Energies of the Group IIIA Elements (20)

<u>Bond</u>	<u>Bond Energy (kcal/mole)</u>
B-Cl	127
Al-Cl	117.1
Ga-Cl	113.5
In-Cl	102.4
Tl-Cl	89.6

TABLE IVPauling Radii of the Group IIIA Elements

<u>Ion</u>	<u>Radius (\AA)</u>	<u>Ion</u>	<u>Radius (\AA)</u>
B^+	-	B^{+3}	0.20
Al^+	-	Al^{+3}	0.50
Ga^+	1.13	Ga^{+3}	0.62
In^+	1.32	In^{+3}	0.81
Tl^+	1.40	Tl^{+3}	0.95

Although formation of the B-Cl bond is favorable, electrochemical oxidation of boron in the LiCl-KCl eutectic melt does not take place because of the high ionization potentials of that element. The trend of the standard potentials of the $M(\text{III})/M(0)$ and $M(\text{III})/M(\text{I})$ redox couples can be attributed to the decreasing stability of the M-Cl bond in going down the group. The standard potential of the $\text{Tl}(\text{III})/\text{Tl}(\text{I})$ redox couple is over one volt more positive than the corresponding indium potential. A clue to this behavior can be obtained from the fact that $\text{InCl}_3(\text{s})$ is 84 kcal/mole more stable than is $\text{InCl}(\text{s})$ (21), and that $\text{TlCl}_3(\text{s})$ is only 34 kcal/mole more stable than $\text{TlCl}(\text{s})$ (22). On the basis of the postulated trend of bond energies, it would seem that the standard electrode potential of the $\text{In}(\text{I})/\text{In}(0)$ couple would be more negative than that of the $\text{Tl}(\text{I})/\text{Tl}(0)$ couple. The opposite behavior is observed and this can be explained by the fact that the first ionization potential of thallium is greater than the first ionization potential of indium (Table II). The energy required to ionize thallium, then, is greater than the energy released in the formation of the chloro-thallium complex.

It must be emphasized that the explanation given above for the trend of the standard potentials of the group IIIA elements is a simplified one. In essence, the following reaction is being examined when the standard electrode

potential of an $M(n)/M(0)$ (n represents the oxidation number of the metal) redox couple is determined in the $LiCl-KCl$ eutectic melt:



The standard change in free energy of this reaction is given by the relationship:

$$\Delta G^\circ = 2(G^\circ_{M(n)} - G^\circ_{M(0)}) - n(G^\circ_{Pt(0)} - G^\circ_{Pt(II)}) .$$

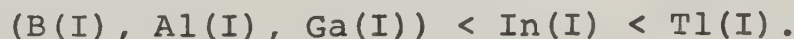
Since the free energy change expressed by $G^\circ_{Pt(0)} - G^\circ_{Pt(II)}$ is defined to be zero, the change in free energy expressed by $G^\circ_{M(n)} - G^\circ_{M(0)}$ defines the standard potential of the redox couple. At this point, it should be emphasized that $M(n)$ represents the solvated ion in solution. The following reactions will determine the value of $G^\circ_{M(n)} - G^\circ_{M(0)}$:

<u>Reaction</u>	<u>Energy Involved</u>
$M \rightarrow M_{(g)}$	Free energy of formation of the monatomic gaseous element.
$M_{(g)} \rightarrow M(n)_{(g)}$	$\sum_{i=1}^n (I.P.)_i$, I.P. = ionization potential.
$M(n)_{(g)} + MCl_x^{n-x}$	Free energy of solvation.

The free energy of solvation of an ion cannot be experimentally determined, but its value can be calculated if the standard electrode potential of the $M(n)/M(0)$ redox

couple is known. The calculation of a series of values for the free energies of solvation of various ions independent of the $M(n)/M(0)$ standard electrode potential is not possible, and as a result, the trend in the values of the free energies of solvation is necessarily self-consistent with the standard electrode potentials to be examined.

The species $Al(I)$ and $Ga(I)$ do not exist in the $LiCl-KCl$ eutectic melt and therefore the standard electrode potentials of the $Al(I)/Al(0)$ and $Ga(I)/Ga(0)$ couples must be greater than -1.762 V ($E^\circ, Al(III)/Al(0)$) and -1.141 V ($E^\circ, Ga(III)/Ga(0)$), respectively. As a result, the equilibrium constants of the hypothetical reactions $3Al(I) \rightleftharpoons Al(III) + 2Al(0)$ and $3Ga(I) \rightleftharpoons Ga(III) + 2Ga(0)$ must be greater than unity. From the equilibrium constants of the reactions $3In(I) \rightleftharpoons 2In(0) + In(III)$ ($K = 1.46 \times 10^{-4} \text{ l}^2 \text{ mol}^{-2}$) and $3Tl(I) \rightleftharpoons 2Tl(0) + Tl(III)$ ($K = 2.55 \times 10^{-23} \text{ l}^2 \text{ mol}^{-2}$), it is apparent that $In(I)$ is much less stable in the eutectic melt than is $Tl(I)$. Thus the stability of the $M(I)$ oxidation state of the group IIIA elements in the $LiCl-KCl$ eutectic melt is:



This trend in the stability of the $M(I)$ oxidation state is also followed in a tetrachloroaluminate melt for $Ga(I)$, $In(I)$, and $Tl(I)$, as was shown by Anders and Plambeck (10).

The equilibrium constants for the reactions $3\text{Ga(I)} \rightleftharpoons 2\text{Ga(0)} + \text{Ga(III)}$, $3\text{In(I)} \rightleftharpoons 2\text{In(0)} + \text{In(III)}$, and $3\text{Tl(I)} \rightleftharpoons 2\text{Tl(0)} + \text{Tl(III)}$ in that melt are 1.00×10^{-14} , $<6.9 \times 10^{-28}$, and $<1.10 \times 10^{-51} \text{ l}^2 \text{ mol}^{-2}$, respectively. These values show that the tetrachloroaluminate melt stabilizes the M(I) oxidation state, relative to the M(III) state, to a greater degree than does the LiCl-KCl eutectic melt. While Tl(III) is a stable entity in the fused LiCl-KCl eutectic, it does not exist in the tetrachloroaluminate melt. It should also be pointed out that In(0) and Tl(0) are not stable in the tetrachloroaluminate melt, as they are quantitatively oxidized to In(I) and Tl(I) by Al(III).

C O N C L U S I O N

Elemental boron cannot be coulometrically oxidized in the fused LiCl-KCl eutectic. Aluminum metal can be anodized to Al(III). Although the existence of Ga(I) and In(I) compounds has been shown, only In(I) exists in the LiCl-KCl eutectic melt. The other stable oxidation states of gallium and indium in the melt are Ga(0), Ga(III), In(0), and In(III). Thallium metal can be electrolytically oxidized to Tl(I), which in turn can be oxidized to Tl(III). The standard electrode potentials between different oxidation states of the same element have been established. From a preparative point of view, this study has introduced a novel method for the preparation of the anhydrous chlorides of gallium and indium.

B I B L I O G R A P H Y

1. H. A. Laitinen and C. H. Liu, J. Amer. Chem. Soc., 80, 1015 (1958).
2. E. R. Van Artsdalen and I. S. Yaffe, J. Phys. Chem., 59, 118 (1955).
3. S. Asakura and T. Mukaibo, Electrochim. Acta, 13, 881 (1968).
4. A. De Haan and H. Vander Poorten, C. R. Acad. Sci., Paris, Ser. C, 261, 5462 (1965).
5. Y. Pointud, J. Hladik, and G. Morand, C. R. Acad. Sci., Paris, Ser. C, 269, 955 (1969).
6. H. A. Laitinen, R. P. Tischer, and D. K. Roe, J. Electrochem. Soc., 107, 546 (1960).
7. S. Asakura and T. Mukaibo, J. Electrochem. Soc. Japan, 35, 188 (1967).
8. H. A. Laitinen and J. W. Pankey, J. Amer. Chem. Soc., 81, 1053 (1959).
9. J. A. Plambeck and J. Chapman, unpublished work.
10. U. Anders and J. A. Plambeck, Can. J. Chem., 47, 3055 (1969).
11. J. H. R. Clarke and R. E. Hester, Inorg. Chem., 8, 1113 (1969).
12. G. Delarue, J. Electroanal. Chem., 1, 285 (1959).
13. H. A. Laitinen, W. S. Ferguson, and R. A. Osteryoung, J. Electrochem. Soc., 104, 516 (1957).

14. D. Inman, G. J. Hills, L. Young, and J. O'M. Bockris, Trans. Far. Soc., 55, 1094 (1959).
15. D. L. Maricle and D. N. Hume, J. Electrochem. Soc., 107, 354 (1960).
16. Copy of FORTRAN program used is available in the Appendix to the Ph.D. thesis of F. G. Bodewig, University of Alberta, Edmonton, Alberta, 1970.
17. R. K. McMullen and J. D. Corbett, J. Amer. Chem. Soc., 80, 4761 (1958).
18. R. J. Clark, E. Griswold, and J. Kleinberg, J. Amer. Chem. Soc., 80, 4764 (1958).
19. NSRDS-NBS 34, U.S. Government Printing Office, Washington D. C., pp.2-4 (1970).
20. R. F. Barrow, Trans. Far. Soc., 56, 952 (1960).
21. NBS Circular 500-Part I. U. S. Government Printing Office, Washington, D. C., p.171 (1961).
22. NBS Circular 500-Part I. U. S. Government Printing Office, Washington, D.C., p.174 (1961).

PART II
THE ELECTROCHEMISTRY OF THE GROUP IVA ELEMENTS
IN FUSED LiCl-KCl EUTECTIC

A B S T R A C T

Carbon (graphite) is electrochemically inert in the fused LiCl-KCl eutectic at 450°C. Attempts to anodize silicon into the LiCl-KCl eutectic melt are hindered by a complex phenomenon called the "anode effect", and no electroactive species of silicon were found in the melt.

The standard electrode potentials of the Ge(II)/Ge(0) and Ge(IV)/Ge(II) redox couples in the fused LiCl-KCl eutectic at 450°C are -0.792 V and -0.665 V versus the standard molar platinum reference electrode (s.m.p.e.). A voltammetric study of Ge(II) showed that potentials more negative than -0.80 V were sufficient for the electrodeposition of germanium. Chronopotentiometric reduction of Ge(II) on gold follows the Sand equation and gives evidence of alloy formation. The cell Au-Ge (12 wt.% Ge, l)/Ge(II) in LiCl-KCl/Ge(s) was studied, and the following parameters were determined for the alloy: $\Delta S_f^\circ = 14.2$ e.u.; $\Delta G_f^\circ = -1.24$ kcal/mole; and $\Delta H_f^\circ = +9.00$ kcal/mole. Optical and scanning electron metallographic studies were made of germanium deposited onto a gold substrate.

The standard electrode potentials of the Sn(II)/Sn(0) and Pb(II)/Pb(0) redox couples were found to be -1.079 V

and -1.093 V versus the s.m.p.e. respectively, in agreement with earlier work. The standard potential of the Sn(IV)/Sn(II) redox couple is -0.310 V. Pb(II) cannot be oxidized to Pb(IV) in the fused LiCl-KCl eutectic.

I N T R O D U C T I O N

Carbon

Graphite (carbon) is electrochemically inactive in the fused LiCl-KCl eutectic. Attempts to anodize carbon result in chlorine evolution (the limiting anodic reaction in the melt), and electrolytic reduction of carbon results in lithium deposition (the limiting cathodic reaction in the melt). Thus, graphite has been used in electrochemical investigations as a counter electrode or an inert electrode for the oxidation (or reduction) of an electroactive species from one oxidation state to another. Morris and Harry (1) formed anodic deposits of carbon by the electrolysis of fused calcium carbide-lithium chloride and lithium carbide-calcium chloride mixtures, and found that the current efficiency for the process was close to 100% based on the oxidation of the acetylide ion (C_2^{-2}). Although calcium carbide is soluble in the LiCl-KCl eutectic melt, attempts by Plambeck (2) to deposit carbon from it were not successful. Barde, Buvet, and Dubois (3) carried out voltammetric studies in the fused LiCl-KCl eutectic and reported the anodic oxidation of carbon monoxide and of some hydrocarbons.

Silicon

Investigations by the present author have shown that silicon does not react with the fused LiCl-KCl eutectic;

this observation is in accord with that of Delarue (4) who reported the insolubility of silicon in the melt. A phenomenon known as the "anode effect" (5,6) was observed by the present author when attempts were made to anodize silicon. Cathodization of silicon results in lithium deposition. Attempts to reduce silicon tetrachloride in the eutectic melt at a platinum electrode resulted in lithium deposition.

Panzer (7) studied a series of miniature cells ("pill cells") of the type $\text{Mg/MgO/LiCl-KCl/kaolin/LiCl-KCl/A}$, where the LiCl-KCl eutectic was initially pressed into a "pill" 1-3 mm in height and 1 cm in diameter. The Mg/MgO electrode served as the reference electrode; kaolin, a clay, prevented the anolyte and catholyte from mixing; and A was the metal anode whose standard potential was to be estimated. No compounds of Mg(II) or A(n) (n being the oxidation number of A) were added to the catholyte or anolyte. Although magnesium oxide is virtually insoluble in the fused LiCl-KCl eutectic at 450°C , a small concentration of Mg(II) will exist in solution. The presence of A(n) in the melt must have arisen from oxidation of A by melt impurities. If the Mg(II) and A(n) concentrations were approximately equal, then the open circuit potential of the cell would approximate the standard potential of the system A(n)/A . Using this approach, Panzer (7) obtained a value of -0.35 V for the potential of silicon

against platinum. This value was not ascribed to any specific redox couple of silicon.

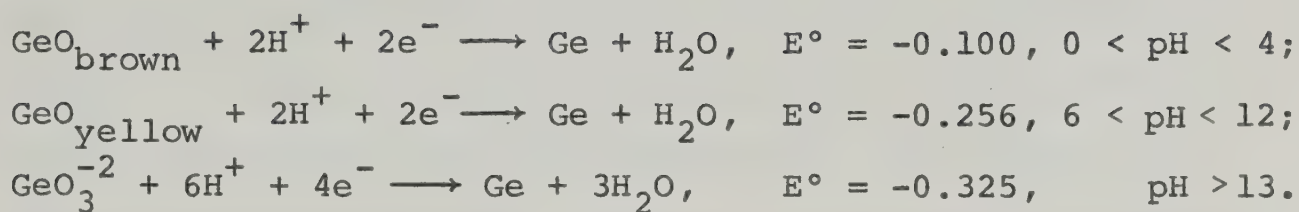
Germanium

The electrochemistry of germanium stems from the time of its discovery by Winkler (8) who, in 1886, electrolyzed aqueous ammonia-ammonium tartrate solutions of germanium dioxide. Further work into the aqueous electrochemistry of germanium was carried out by Tainton and Clayton (9), who discovered that the electrolytic production of zinc was seriously affected by co-electrodeposition of small quantities of germanium. They ascribed this adverse effect to the low overpotential of hydrogen on a germanium surface. This observation was verified by Hall and Koenig (10). Schwarz, Heinrich, and Hollstein (11) attempted to develop a quantitative procedure for the electrodeposition of germanium from aqueous media. An exhaustive study was made into solution composition (e.g., use of complexing agents, acidic media, basic media, etc.), temperature, and current density employed for the electrolyses, and it was found in all cases that germanium deposition took place only to a limited extent and was then followed by hydrogen evolution. A similar study by Fink and Dokras (12) again demonstrated that the electrodeposition of germanium from aqueous media is limited to thin flashes of the metal, because the overpotential of hydrogen on germanium is low. Land (13) showed that germanium could be uniformly deposited

onto a platinum surface freshly plated with copper, but once the copper cathode was completely covered, hydrogen evolution occurred.

Jirsa (14) reported that germanium can be quantitatively anodized to Ge(IV) in both acidic and basic media. He proposed that concentration polarization of the germanium anode in prolonged electrolysis caused the reaction $\text{Ge(IV)} + \text{Ge(0)} \rightleftharpoons 2\text{Ge(II)}$ to occur (i.e., Ge(IV) produced reacted with the germanium anode), and that subsequent hydrolysis of Ge(II) resulted in the formation of a layer of GeO on the germanium anode. However, Sullivan, Klein, Finne, Pompliano, and Kolb (15), and Reid (16) have shown that the current efficiency for the reaction $\text{Ge(0)} \longrightarrow \text{Ge(IV)} + 4\text{e}^-$ exceeds 100%, and thus anodization of germanium results in the formation of Ge(IV) and Ge(II), the latter being hydrolyzed to produce GeO.

Nichols and Cooper (17) concluded that the GeO_2/Ge couple is not reversible in aqueous media. Using thermodynamic data, Lovrecek and Bockris (18) have calculated the standard electrode potentials of twenty-three possible redox couples involving germanium in aqueous media. Of these, they found that the following three redox couples describe the thermodynamics of germanium in aqueous media, since they were the only couples that could be correlated to the experimental data obtained:



The low overpotential of hydrogen on germanium led to the idea that electrodeposition of germanium from non-aqueous media, i.e., media where the hydrogen ion concentration is very small or nonexistent, would yield better germanium deposits. Most work in organic media has employed polyalcohols, mainly ethylene and propylene glycol, as the solvent, and the germanium compounds most often used with these solvents to electrodeposit germanium have been germanium tetrachloride and germanium tetraiodide. Thus, Fink and Dokras (12) were able to obtain good deposits of germanium from an ethylene glycol-germanium tetraiodide mixture. However, there were difficulties with this solution, such as considerable solvent loss at the operating temperature. A more efficient method of plating germanium was proposed by Szekely (19). He electrodeposited germanium from solutions of germanium tetrachloride in ethylene glycol and germanium tetrachloride in propylene glycol and found the latter to give a superior deposit of germanium. Szekely (19) also studied the anode current efficiency for the oxidation of germanium in ethylene glycol and found that the current efficiency of the reaction $\text{Ge}(0) \longrightarrow \text{Ge}(\text{IV}) + 4\text{e}^-$ exceeded 100%, and thus concluded that the germanium anode

must also be oxidized to Ge(II). Attempts by the present author to anodize germanium in sulfolane (tetrahydrothiophene 1-1 dioxide) were not successful. The absence of germanium in any oxidized form was confirmed by voltammetry. The present author also found germanium dioxide and germanium tetrachloride to be insoluble in sulfolane.

Organic media, then, have been found to be more conducive to the production of germanium deposits than aqueous media. This is a result of the nonavailability of hydrogen ions in organic media, which has the effect of increasing the hydrogen overpotential on germanium to the extent where germanium deposition is the favored reaction. It is also very likely that germanium tetrahalide-alcohol complex formation aids in the electrodeposition process. This is analogous to the situations which exist in aqueous media where metal complexation leads to a better deposit, as in the deposition of silver from solutions of $\text{Ag}(\text{CN})_2^-$ and $\text{Ag}(\text{aq})^+$, the former giving a better deposit than the latter.

The first attempt to electrodeposit germanium from fused salt media was carried out by Tressler and Dennis (20), who plated germanium from germanium dioxide dissolved in molten fluoride baths. Their germanium yields were low due to the loss of germanium monoxide, an intermediate compound formed in the electrolysis. Electrolysis of fused salt baths consisting of equimolar amounts of potassium and

sodium carbonates in which germanium dioxide had been dissolved was carried out by Hall and Koenig (10). They used a platinum cathode and found that the deposited germanium alloyed with the cathode. Fink and Dokras (12) electrolyzed solutions of germanium dioxide in fused sodium tetraborate. This fused solvent was found to be satisfactory, as germanium monoxide, formed in the reduction of germanium dioxide, was soluble in the melt and hence led to higher current efficiencies for the germanium deposition. Fink and Dokras (12) related the current efficiency of germanium production to experimental conditions on the basis of the sodium film theory proposed by Fink and Ma (21). According to this theory, increases in current efficiency above 900°C are attributable to the production of a sodium vapor film on the cathode surface (sodium metal boils at 883°C). Thus reduction of Ge(IV) takes place via the secondary reaction:

$$\text{Ge(IV)} + 4\text{Na(0)}(\text{g}) \longrightarrow \text{Ge(0)} + 4\text{Na(I)}.$$

Barbier-Andrieux (22) reported an extensive investigation of the preparation of germanium from fused salt solutions of germanium dioxide, and described the successful electrowinning of germanium from fused $\text{Na}_2\text{O} \cdot 2\text{GeO}_2$ and from germanium dioxide dissolved in silicate melts. The purity of germanium obtained was greater than 99%. Similar studies by Andrieux and Barbier-Andrieux (23) described germanium production from germanium dioxide dissolved in fused borate, silicate, phosphate, and sodium oxide-sodium

fluoride melts. Bockris, Diaz, and Green (24) reported conditions for the production of germanium dendrites at a graphite cathode by the electrolysis of a sodium tetraborate-germanium dioxide melt.

Delimarskii, Bojko, and Schilina (25) carried out a voltammetric study of germanium dioxide dissolved in molten borax and found that Ge(IV) is reversibly reduced according to the equation $\text{Ge(IV)} + 4e^- \longrightarrow \text{Ge(0)}$. A voltammetric study of germanium dioxide dissolved in fused sodium metaphosphate (at 680°C) was undertaken by Kaptsova and Delimarskii (26). They showed that germanium dioxide is reduced in two stages in that melt: at a half-wave potential of -0.73 V (probably with respect to an oxygen reference electrode) Ge(IV) was reduced to Ge(II), while at a half-wave potential of -0.82 V reduction of Ge(IV) to the metal took place. Monnier and Tissot (27) studied the electrolysis of germanium dioxide in a fused fluoride melt, and obtained germanium in purity greater than 99.9%. They postulated the mechanism of the electrolysis to be the discharge of Ge(IV) and O^{2-} formed from the dissociation of germanium dioxide. Rius, Colom, and Artracho (28) studied the electrowinning of germanium from solutions of germanium dioxide in fused borate and silicate melts. They proposed that germanium deposition proceeded through the reduction of germanium ions by alkali metals, the ions of which were previously reduced at the cathode. This corresponds to the sodium

film theory expounded by Fink and Ma (21). Verdieck and Yntema (29) found that it was possible to obtain a thin plate of germanium, at 156°C , from a tetrachloroaluminate melt containing potassium fluorogermanate. This temperature was much lower than those previously employed for the electrodeposition of germanium. Two reduction potentials were reported with respect to an aluminum reference electrode immersed in the melt: (a) $+0.50\text{ V}$ at low current densities, and (b) -0.01 V at large current densities, germanium deposition occurring at this potential. Although the authors do not ascribe any processes to these potentials, it is most likely that at low current densities ($+0.50\text{ V}$), reduction of Ge(IV) to Ge(II) occurred, whereas at large current densities (-0.01 V) the potential was sufficient to cause both reduction of Ge(IV) to metallic germanium, as well as reduction of Al(III) to Al(0) . The only other study reporting a potential value for germanium in fused salt media is given by Panzer (7) who reported the potential for germanium (versus the s.m.p.e.) in the fused LiCl-KCl eutectic (at 450°C) as being -0.89 V . As in the case of silicon, he did not state to which redox system this value corresponded. Seo (30) has patented a method for the cathodic deposition of germanium from germanium tetrafluoride added to a fluoride melt. Polishing (anodization) of germanium has been accomplished by Brouillet and Epelboin (31) in mixtures of fused sodium chloride-potassium

chloride and potassium chloride-magnesium chloride.

While previous fused salt work with germanium has almost completely employed high temperatures (in excess of 800°C) and germanium dioxide as the source of germanium, the present author has found that the electrochemistry of germanium could be studied in the fused LiCl-KCl eutectic, at the much lower temperature of 450°C. Solutions of Ge(II) were produced by the anodization of metallic germanium, and this species was further oxidized to germanium tetrachloride at a graphite electrode. Germanium dioxide was found to be insoluble in the LiCl-KCl eutectic melt. It was possible to electrodeposit germanium from the divalent state. Extended electrolysis of Ge(II), either constant current electrolysis using gold or platinum cathodes or constant potential electrolysis using a gold cathode, led to the formation of black, bulky, non-adherent deposits of germanium. These deposits, however, were found to contain some germanium dendrites. Because the electrodeposition of germanium in the LiCl-KCl eutectic was carried out at 450°C, the alkali metal gas film theory proposed by Fink and Ma (21) cannot explain the reduction of Ge(II). A potentiometric study by the present author has shown that the Ge(II)/Ge(0) redox couple obeys the Nernst equation in the fused LiCl-KCl eutectic at 450°C. Thus, the Ge(II)/Ge(0) system is reversible in

this melt, and reduction of Ge(II) takes place via the reaction $\text{Ge(II)} + 2\text{e}^- \longrightarrow \text{Ge(0)}$.

Tin

Tin is liquid at the standard operating temperature of the fused LiCl-KCl eutectic, 450°C. The standard electrode potential of the Sn(II)/Sn(0) couple has been determined by Laitinen and Liu (32) to be -1.082 ± 0.002 V. Delarue (4) has reported -1.1 V as the half-wave potential for the voltammetric reduction of Sn(II) at a platinum electrode, in agreement with this value of the standard potential of the Sn(II)/Sn(0) redox couple. Delarue (4) also studied the voltammetric oxidation of Sn(II) to Sn(IV) at a graphite electrode and reported the half-wave potential of this process to be 0.0 V. The present author determined the standard potential of the Sn(IV)/Sn(II) couple to be -0.310 ± 0.003 V, and a voltammetric study of the oxidation of Sn(II) to Sn(IV) at a graphite electrode showed the half-wave potential of the process to be -0.31 V. The difference in half-wave potential values for Sn(II) oxidation may be attributed to Delarue's use of wet melts (4), or use of large current densities and long electrolysis times in obtaining voltammetric data (33). No reaction between tin and the LiCl-KCl eutectic melt was observed.

Lead

Lead, like tin, is liquid at 450°C (the operating temperature of the fused LiCl-KCl eutectic). The standard potential of the Pb(II)/Pb(0) redox couple was determined by Laitinen and Liu to be -1.101 ± 0.002 V (32). A voltammetric study by Delarue (4) showed that the half-wave potential of the reduction of Pb(II) at a platinum electrode is -1.1 V, in agreement with this standard potential of the Pb(II)/Pb(0) couple. Delarue (4) also showed that dissolution of lead (II) oxide in the LiCl-KCl eutectic melt produces Pb(II) and O^{-2} ; PbO_2 and Pb_3O_4 dissolve in the melt to give oxygen gas and Pb(II). This shows that oxidation states of lead greater than Pb(II) do not exist in the melt. The present author attempted to anodize solutions of Pb(II) in the fused LiCl-KCl eutectic at a graphite electrode and observed only chlorine evolution. This again shows that Pb(II) is the highest stable oxidation state of lead in the melt. No reaction between lead and the fused LiCl-KCl eutectic was observed.

E X P E R I M E N T A L

Apparatus

The apparatus employed in Part II of this thesis is basically identical to that described in Part I. In the silicon study, the silicon rod was suspended into the fused LiCl-KCl eutectic by a platinum wire sealed in a Pyrex tube. Silicon tetrachloride was introduced into the melt using a flow of argon, as follows. Liquid silicon tetrachloride was placed into a gas wash bottle, and a gas dispersion tube was immersed into the silicon tetrachloride. Due to the low boiling point of silicon tetrachloride (57.6°C), it was possible to volatilize the silicon tetrachloride by passing argon through it, and then bubbling the resulting mixture into the eutectic. The silicon tetrachloride-argon gas mixture was passed into the melt through a 3 mm Pyrex tube which was sealed with sealing wax, into a standard taper 14/20 joint in the cell head. Cell resistance was measured with an A.C. impedance bridge (Type 1650A, General Radio Co., Concord, Mass.).

For the coulometric oxidation of germanium, a germanium bar was suspended into the melt by a copper wire wound into a groove that was ground near the top of the bar. The indicating electrodes used for voltammetric scans were made of tungsten wire (5 mm long and 0.5 mm in diameter) sealed in uranium glass. Voltammetric scans

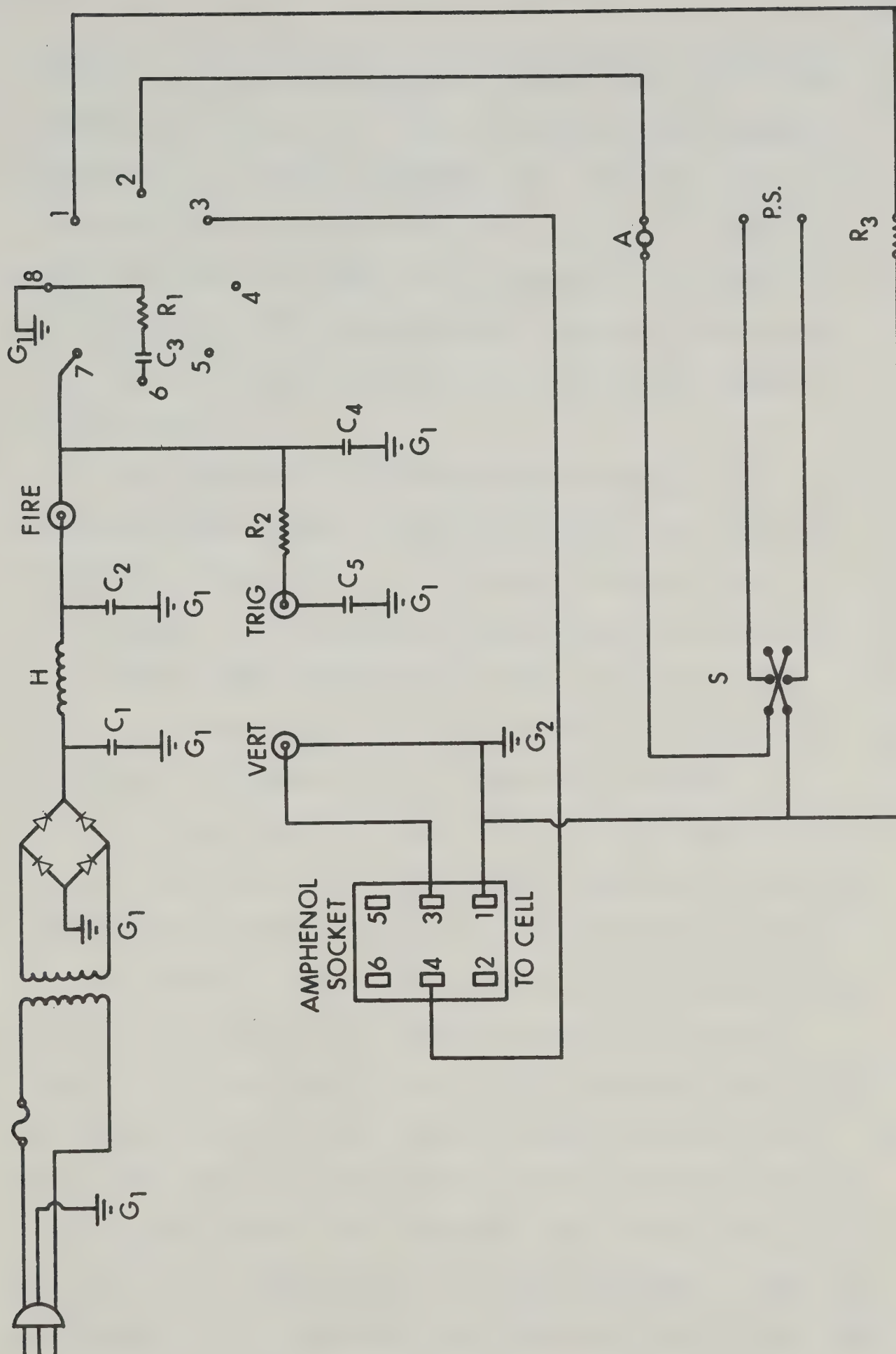
were carried out with a Metrohm-Polarecord E261 polarograph. Constant potential electrolyses were carried out with a Wenking Model 61 RH potentiostat, using gold electrodes. Chronopotentiometric measurements employed a gold foil electrode approximately 0.4 cm^2 in area. (The counter electrode and reference electrodes were, respectively, a carbon rod and a Pt(II)/Pt(0) electrode. Each was housed in a separate isolation compartment). The constant current was obtained from a Hewlett-Packard Model 6525A DC power supply and was controlled by a switching circuit, as shown in Figure 1. A 10 V DC signal, produced by this circuit from the AC main, was used to switch current from the "dummy cell", R_3 , to the electrochemical cell, using a mercury wetted relay (pin numbers 1-8). The RC network between pins 7 and 8 of the mercury wetted relay assured that the oscilloscope was fired before current from the power supply was sent to the electrochemical cell. Traces were recorded on a Model 175A oscilloscope equipped with 1750B and 1781B plug-in units and a 196B camera (Hewlett-Packard), using ASA 3000 Polaroid film.

The gold-germanium alloy (eutectic composition, 12 wt. % germanium (34)) was prepared by placing appropriate amounts of gold and germanium in a quartz boat which had been cleaned by boiling in perchloric acid. The mixture was fused under a flow of argon (dried by passage over magnesium perchlorate) in a Lindberg Hevi-Duty 54032A

FIGURE 1

Switching and Triggering Circuit for
Chronopotentiometry of Germanium

- G_1 . AC main ground.
- G_2 . Power supply ground.
- H. 10 Henry Choke.
- C_1, C_2 . 500 millifarad capacitors.
- C_3 . 500 microfarad capacitor.
- C_4 . 100 picofarad capacitor.
- C_5 . 300 picofarad capacitor.
- R_1 : 7.5 ohm, 5 watt resistor.
- R_2 . 330 ohm resistor.
- R_3 . 10 ohm resistor.
- P.S. Power supply.
- S. Current reversing switch.
- A. Ammeter.
- 1-8. Mercury wetted relay.
- FIRE. Foot switch.
- TRIG. Connection to trigger input of oscilloscope.
- VERT. Connection to signal input of oscilloscope.
- AMPHENOL SOCKET: 1,4: Connection to anode or cathode.
- 3: Connection to reference electrode.



furnace in conjunction with a Lindberg Hevi-Duty 59344 temperature controller. In the thermodynamic study of gold-germanium alloy formation, the alloy was held in a Pyrex cup which was attached to a glass rod. Contact with the alloy was made with a tungsten wire sealed in uranium glass. The germanium bar, used as a reference electrode, was suspended from a platinum wire sealed in a Pyrex tube.

The topography of the germanium deposit on a gold substrate was studied using both optical and scanning electron microscopes: a Carl Zeiss Ultraphot(III) Metallograph, a photographic metallurgical microscope (Carl Zeiss Oberkochen, Wuerth, West Germany) and a Stereoscan S4 scanning electron microscope (Cambridge Scientific Instruments Ltd., Cambridge, England).

Tin and lead are liquid at 450°C, and were anodized from an electrode of the same design employed in the anodization of gallium and indium, as described in Part I of this thesis. The cell head used in the tin study was modified to contain two standard taper 14/20 female joints (one joint being used for the introduction of the reference electrode, the other acting as an inlet for argon gas and the thermocouple), and a standard taper 19/38 female joint. The standard taper 19/38 joint contained the tin compartment which was designed to keep an atmosphere of tin tetrachloride above the melt, since tin

tetrachloride, formed in the oxidation of Sn(II), slowly volatilizes from the melt. This consisted of a Pyrex tube, 10 mm in diameter, which was sealed at one end with a D porosity sintered glass disk, and attached at the other end to a standard taper 19/38 male joint. A side arm above the standard taper 19/38 male joint was joined to a Teflon stopcock; the sidearm led to two gas wash bottles mounted back-to-back, the furthest one from the Teflon stopcock being filled with concentrated sulfuric acid. The top of the tin compartment was fitted with a standard taper 14/20 female joint, into which a Teflon stopper was placed. This stopper had appropriate holes drilled into it to support the tin electrode and to provide an inlet and outlet for the argon gas which was maintained above the melt during the anodization of metallic tin. A static atmosphere was maintained in the compartment during the oxidation of Sn(II). A hole drilled into the cell head served both as an inlet for the graphite counter electrode and an outlet for the argon gas which blanketed the bulk melt.

The apparatus employed in the lead study was identical to that described for indium and gallium in Part I of this thesis.

Procedure

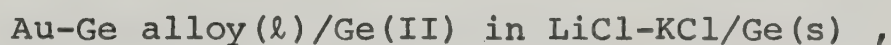
Melt purification, arrangement of the electrochemi-

cal cell, and the procedure employed in carrying out the coulometric oxidations and potential measurements have been described in Part I of this thesis. The germanium rod, and liquid tin and lead pools were anodized to give solutions of Ge(II), Sn(II), and Pb(II), respectively. The Ge(II) and Sn(II) were further oxidized at a graphite electrode to Ge(IV) and Sn(IV) after the germanium and tin electrodes had been removed from their respective isolation compartments. Correction of the calculated standard electrode potential for the thermoelectric potential between platinum and the indicating electrode was made as described in Part I of this thesis.

In order to obtain reproducible voltammetric curves for the germanium system, it was found necessary to hold the tungsten microelectrode at positive (chlorine evolution) potential for a few moments before each scan. This was done in the bulk melt. Similar procedures were found necessary to obtain reproducible chronopotentiometric curves. The solutions of Ge(II) were prepared coulometrically. The gold electrode was anodized until all deposits of germanium were removed, i.e., until chlorine evolution just began. It was necessary to carry out this procedure carefully at a low current density ($<50 \text{ mA/cm}^2$) to avoid appreciable anodization of gold into solution. The electrode was then momentarily anodized at this potential, the current was shut off, and the solution in the compartment

was stirred by rotation of the gold flag electrode. Cathodic chronopotentiometric curves were all run 30 sec. after cessation of the anodic current.

In the thermodynamic study of gold-germanium alloy formation, which was a study of the cell:



the previously prepared LiCl-KCl eutectic was fused and filtered in order to remove any magnesium present, as magnesium ribbon was used in the preparation of the melt. A 0.02 M solution of Ge(II) was prepared in situ by electrolytic anodization of germanium; the resulting solution was thoroughly stirred after cessation of Ge(II) generation. The solution temperature was monitored with a calibrated chromel-alumel thermocouple sheathed in a Pyrex tube. The germanium bar, alloy holder, and thermocouple were placed as close together as possible to minimize thermal gradients. Potential-temperature measurements were made every two hours after a new temperature setting had been made. The experiment was conducted under a static, dry argon atmosphere. The thermoelectric potential between the electrodes was determined in a separate experiment as previously described, and this potential was subtracted from the observed cell potential.

The cross-sectional sample of germanium deposited onto gold used in the optical microscopic examination was

prepared as follows. A brass cylinder (1" in diameter, 1" in length) was placed in a paper cup and a mold was made by pouring a mixture of Silastic A RTV mold-making rubber and Dow Corning Catalyst 1 (Dow Corning Corp., Midland, Michigan) over the cylinder. The mold was cured by heating it at 100°C for 24 hours. A small incision was made into the bottom of the mold and the germanium-plated gold sample was placed edgewise into the incision. The mold was then filled with a mixture of Clear Casting Resin (House of Plastic, Edmonton, Canada) and catalyst (Algonquin Manufacturing Ltd., Toronto, Canada). The plastic was hardened at 100°C for 24 hours. The impregnated sample was then manually ground smooth, starting with a #240 grit, waterproof, adhesive-backed, silicon carbide paper, and progressing to a #600 grit. The sample was then treated on a polishing lap using a 6 μm diamond abrasive and "Compound Thinner" as a lubricant (Micro Metallurgical Ltd., Thornhill, Ont., Canada), and was finally treated on a finishing lap using Linde B (0.05 μm Al_2O_3) suspended in a detergent solution which acted as a wetting agent. No sample etching was carried out. The germanium-plated gold sample was prepared by treating a gold foil in aqua regia, followed by electrolytic polishing in the fused LiCl-KCl eutectic melt. Germanium(II), prepared by the coulometric oxidation of a germanium bar, was plated onto the gold foil at a constant potential of -0.86 V.

The thickness of the germanium plate was determined with a filar micrometer eyepiece attached to a Tukon Tester (Wilson Mechanical Inst. Co., N.Y.) which is used for indentation hardness tests where optical measurement of indentation is to be made.

For the scanning electron microscopy study, the gold foil was cleaned by scrubbing it in one direction with a cotton swab soaked in an aqueous suspension of cerium oxide. This had the effect of streaking the gold surface so that differentiation of the gold underlay from the germanium deposit could be made if the gold surface was not completely coated in the electrodeposition process.

Chemicals and Materials

Silicon rod (1.4 cm diameter, 5 cm long; 99.9999% pure) was obtained from Gallard-Schlesinger, Long Island, N.Y. Silicon tetrachloride was obtained from Fisher Scientific Ltd. Germanium rod (0.25" diameter, 99.99% pure) was obtained from A. D. Mackay Inc., N.Y. The gold used in the thermodynamic study of gold-germanium alloy formation was obtained in bar form from Johnson, Matthey, and Mallory Ltd., Toronto. Tin wire was obtained in purity greater than 99.999% from Alfa Inorganics (Beverly, Mass.). Lead wire was also obtained from Alfa Inorganics and was 99.999% pure. Other chemicals and materials used are described in Part I of this thesis.

R E S U L T S

Silicon

The silicon rod was not well wetted when it was initially placed into the LiCl-KCl eutectic melt. Unusual behavior, both of the potential of the silicon electrode and of the electrode itself, was noted when attempts were made to anodize it. In all cases, the potential of the silicon electrode went to values beyond the anodic potential limit of the melt (+0.3 V). The portion of the silicon electrode immersed in the melt became surrounded by a pocket of gas, and the same region of the electrode was covered with luminous, scarlet-colored sparks. These sparks increased in number and intensity when larger current densities were employed. The sparking probably resulted from passage of current from the electrode, through the gas pocket surrounding it, to the eutectic melt. The nonwetting of the silicon electrode, gas pocket formation, and the large potentials observed during electrolysis have been described for other systems. These phenomena are known as the "anode effect" (5,6).

Increases in the current density at the silicon electrode usually reduced the potential of the silicon electrode. This probably resulted from a decrease in resistance of the electrode as a result of localized heating during the passage of large currents, since silicon is a

semiconductor material. This explanation is reasonable, since the resistance path of the cell:

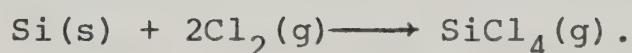


(the graphite electrode was suspended from copper and the silicon electrode was suspended from platinum) was measured to be 1 megohm, which would result in an IR drop of 5 kilovolts during the passage of a 5 mA current through the cell. However, potential drops of approximately 25 V (at 5 mA) were noted, and if this potential is solely attributed to IR drop in the silicon electrode, the electrode resistance would be 5000 ohms. The resistance of the remainder of the cell is negligible compared to this value. After the decrease of the potential of the silicon electrode, resulting from increases in current density, the potential of the silicon electrode then increased as a result of impeded current passage through the large gas pocket that eventually formed around the electrode.

It was occasionally noted that the potential of the silicon electrode during electrolysis decreased from values outside the potential range of the melt, to values within the potential range of the melt. If an oxidized form of silicon was produced during this period, it was not reducible in the melt, since voltammetric scans of the bulk melt and of the solution in which the silicon bar had been electrolyzed were identical, and showed no reduction wave other than

lithium deposition.

Production of white particles (possible SiO_2) accompanied the period of gas pocket formation around the silicon electrode. Because of the large potentials exhibited by the silicon electrode when current was passed through it, it was highly likely that chlorine gas was generated. Chlorine would then react with silicon to produce silicon tetrachloride:



(A similar process was postulated by Mashovets and Alexandrov (35) for the formation of a halide gas film at a carbon anode during the electrolysis of fused sodium chloride). The silicon electrode was introduced into the melt through the top of the outer Pyrex container (see Figure 1 in Part I of this thesis), because the silicon bar was too large to be introduced into the cell through one of the standard taper 14/20 joints in the cell head. As a result, it was necessary to remove the cell head from the outer Pyrex container - thereby exposing the system to the atmosphere. The presence of water vapor in the melt, probably caused by atmospheric contamination of the melt, would result in SiO_2 formation:



White particle production was also noted when $\text{SiCl}_4(\text{g})$ was

bubbled into the melt. Because of the nature of the apparatus employed to introduce $\text{SiCl}_4(\text{g})$, atmospheric contamination of the melt could not be completely avoided, so that water vapor introduced into the melt would react with the $\text{SiCl}_4(\text{g})$ as described.

Identification of the gas evolved at the silicon electrode by mass spectrometry was not successful, as water could not be completely removed from the break-seal tube in which the gas was collected, and was present in the mass spectrum. However, due to the similar behavior of the gas produced during the passage of current through the silicon electrode, and that of silicon tetrachloride bubbled into the melt (viz., "white particle production", non-wetting of the silicon electrode and inner walls of the silicon isolation compartment), it is postulated that $\text{SiCl}_4(\text{g})$ is produced when silicon is anodized in the LiCl-KCl eutectic melt.

Attempts to cathodize silicon into solution were not successful, as the potential exhibited by the silicon electrode showed that lithium deposition was taking place.

When silicon tetrachloride was bubbled around the silicon electrode, the electrode maintained a stable potential of -0.31 V, in agreement with the potential reported by Panzer (7) for silicon. Momentary anodization of the electrode caused the potential of the electrode to go to values far beyond the anodic potential limit of the melt.

This same phenomenon occurred when silicon was anodically polarized in the absence of silicon tetrachloride. Momentary cathodization of the electrode caused the potential of the silicon electrode to go to values beyond the cathodic potential limit of the melt, potentials at which lithium deposition must have taken place. The silicon electrode did not reach an equilibrium potential after either polarization, nor were the values of the electrode potentials after each polarization comparable to one another five minutes after current cessation. Repeated momentary anodizations and cathodizations resulted in the same observations. Thus, the silicon/silicon tetrachloride couple represents an irreversible system in the fused LiCl-KCl eutectic.

The reduction of silicon tetrachloride in the fused LiCl-KCl eutectic was also attempted. Beyond the normal melt preparation, the melt in the silicon compartment was further purified by constant potential electrolysis at -2.0 V, using a large platinum cathode. Silicon tetrachloride was introduced into the melt in a stream of argon gas, and was made to pass over a different platinum cathode held at a potential of -2.15 V. No visible change of the platinum surface took place at this potential. The potential of the platinum cathode was then shifted to -2.75 V, and prolonged electrolysis at this potential resulted in darkening of the platinum. When the platinum electrode had been

removed from the eutectic melt, washed free of adhering salt, and immersed in concentrated hydrochloric acid, gas evolution (H_2) took place. Introduction of the electrode into a bunsen burner flame caused scarlet coloration of the flame. Thus lithium was deposited onto the platinum electrode. It is therefore concluded that reduction of silicon tetrachloride is not possible in the fused $LiCl-KCl$ eutectic.

Germanium

Potentiometry

A total of twenty-seven concentration-potential data points were obtained from four separate coulometric oxidations of the germanium bar electrode at $450^\circ C$. The concentration of $Ge(II)$ ranged from 0.001 to 0.1 M . The current density employed was approximately 2 mA/cm^2 . A plot of the cell potential as a function of the logarithm of the $Ge(II)$ concentration was linear and had a slope of $0.075 \pm 0.006 \text{ V/log unit}$, in agreement with the theoretical value of 0.072 V/log unit expected for a two-electron process at this temperature. The potentials became stable rapidly, usually within five minutes after cessation of electrolysis and gentle stirring. The standard potential of the $Ge(II)/Ge(0)$ couple was calculated as described for gallium and indium in Part I of this thesis, and is $-0.792 \pm 0.008 \text{ V}$.

Further coulometric oxidation of $Ge(II)$ solutions at

a graphite electrode produced visible bubbles at the electrode at polarization potentials significantly less than that of chlorine evolution, suggesting the formation of volatile germanium tetrachloride (b.p., 84°C). The standard potential of the Ge(IV)/Ge(II) redox couple was determined as follows.

The Nernst equation for the reaction $\text{Ge(IV)}_s + 2e^- \rightarrow \text{Ge(II)}_s$, where s represents the species in solution, is

$$E = E^{\circ'} - \frac{RT}{nF} \ln \frac{a_{\text{Ge(II)}}_s}{a_{\text{Ge(IV)}}_s}, \text{ where } E^{\circ'} \text{ is the thermodynamic}$$

standard potential. This equation can be expanded to:

$$E = E^{\circ'} - \frac{RT}{nF} \ln a_{\text{Ge(II)}}_s + \frac{RT}{nF} \ln a_{\text{Ge(IV)}}_s \quad (1)$$

However, the Ge(IV) produced in the melt volatilizes from it, and thus the equilibrium reaction $\text{Ge(IV)}_s \rightleftharpoons \text{Ge(IV)}_g$ exists. (The subscript g represents the gaseous state of Ge(IV) which is GeCl_4). The equilibrium constant for this reaction is $K = a_{\text{Ge(IV)}}_g / a_{\text{Ge(IV)}}_s$, and substitution of this relationship into equation (1) for $a_{\text{Ge(IV)}}_s$, as well as replacing $a_{\text{Ge(II)}}_s$ by $[\text{Ge(II)}]\gamma_{\text{Ge(II)}}$, where $\gamma_{\text{Ge(II)}}$ is the activity coefficient of Ge(II), yields equation (2):

$$E = E^{\circ'} - \frac{RT}{nF} \ln [\text{Ge(II)}] + \frac{RT}{nF} \ln \frac{a_{\text{Ge(IV)}}_g}{K\gamma_{\text{Ge(II)}}} \quad (2)$$

which may be expanded to the following relationship:

$$E = E^{\circ'} - \frac{RT}{nF} \ln [\text{Ge(II)}] + \frac{RT}{nF} \ln a_{\text{Ge(IV)}}_g - \frac{RT}{nF} \ln K\gamma_{\text{Ge(II)}} \quad (3)$$

Since the Nernst plot for the Ge(II)/Ge(0) couple was linear, $\gamma_{\text{Ge(II)}}$ is a constant, and the last term in equation (3) may be incorporated into E° to give

$$E = E^\circ - \frac{RT}{nF} \ln [\text{Ge(II)}] + \frac{RT}{nF} \ln a_{\text{Ge(IV)}}_g \quad (4).$$

If the activity of germanium tetrachloride gas remains constant during the oxidation of Ge(II), a plot of E as a function of $-\ln [\text{Ge(II)}]$ will be linear.

The potential of the graphite electrode drifted in the negative direction after cessation of the electrolysis current in the oxidation of Ge(II). This behavior is to be expected as a result of loss of germanium tetrachloride as the gas (see equation (4)). By taking potential readings as rapidly as possible, the problem of potential drift could be reduced, but not avoided. Using eight data points obtained in two separate experiments under the best possible conditions, and taking the activity of germanium tetrachloride gas to be unity throughout, it was found that linear curves were obtained upon plotting E as a function of $-\ln [\text{Ge(II)}]$. The average slope of these two plots was 0.088 ± 0.002 V/log unit, which is indicative of a two-electron process at 450°C . The theoretical slope for a two-electron process at this temperature is 0.072 V/log unit. Because germanium tetrachloride gas was continuously lost from the surface of the electrode during the oxidation of Ge(II), and during the

period of potential measurements, the assumption of unit $\text{GeCl}_4(\text{g})$ activity throughout the experiment is not completely valid. However, this assumption is a good approximation, because a variation in the activity of $\text{GeCl}_4(\text{g})$ from unity by not more than 5% results in linear plots of E versus $-\ln [\text{Ge(II)}]$, with slopes equal to 0.072 V/log unit. Thus, defining the standard state of germanium tetrachloride gas produced from the oxidation of Ge(II) at 450°C to be unit activity, and setting the prelogarithmic term of equation (4) equal to that of a two-electron process, equation (4) becomes: $E = E^\circ - 0.0717 \log [\text{Ge(II)}]$. Using this equation, the standard potentials calculated for the $\text{Ge(IV)}/\text{Ge(II)}$ couple are: -0.664, -0.666, -0.664, -0.667 V, Run 1; and -0.666, -0.667, -0.665, -0.663 V, Run 2. These values are corrected for the thermoelectric potential of +0.004 V between platinum and graphite at 450°C , and are given in order of increasing germanium tetrachloride gas evolution. The average value for the standard potential of the $\text{Ge(IV)}/\text{Ge(II)}$ redox couple is -0.665 V with a standard deviation of 0.002 V.

From these values of the standard potentials of the $\text{Ge(II)}/\text{Ge(0)}$ and $\text{Ge(IV)}/\text{Ge(II)}$ redox couples, the standard potential of the $\text{Ge(IV)}/\text{Ge(0)}$ redox couple was calculated to be -0.728 ± 0.008 V, and the equilibrium constant for the reaction $2\text{Ge(II)} \rightleftharpoons \text{Ge(0)} + \text{Ge(IV)}$ was calculated to be $1.69 \times 10^{-2} \text{ l mol}^{-1}$. The standard potentials of germanium

on the molar, molal, and mole fraction scales are tabulated in Table I below.

TABLE I

Standard Potentials of Germanium Couples

<u>Couple</u>	<u>E°_{molar}</u>	<u>E°_{molal}</u>	<u>E°_x</u>	<u>Standard Deviation</u>
Ge(II)/Ge(0)	-0.792	-0.792	-0.792	0.008
Ge(IV)/Ge(II)*	-0.665	-0.681	-0.771	0.002
Ge(IV)/Ge(0) [†]	-0.728	-0.736	-0.781	0.008

* Based on a two-electron process.

† Calculated from experimental free energies.

Attempts to cathodize germanium metal into solution were not successful. The only reaction observed was lithium deposition onto germanium, at approximately the standard potential of the Li(I)/Li(0) couple (32).

Voltammetry

A voltammetric scan of the electrolyte alone, using a tungsten microelectrode (which had initially been held at chlorine evolution potential) as the indicating electrode, showed a limiting anodic current at about +0.2 V (chlorine evolution), a limiting cathodic current at -2.6 V (lithium deposition), and a sharp cathodic peak at -0.56 ± 0.05 V. This cathodic peak was not due to melt impurities but was

highly sensitive to electrode treatment and history. Elimination of the pre-scan anodization reduced the peak to about 5% of its previous value. This peak is attributed to the reduction of adherent insoluble polymeric chloride films (36) formed when the tungsten microelectrode was anodized in the bulk melt.

Addition of Ge(II) to the melt (by anodization of a germanium rod) produced an additional cathodic wave whose half-wave potential was -0.76 V, in reasonable agreement with the standard potential, -0.79 V, of the Ge(II)/Ge(0) couple, as shown in Figure 2. The wave height increased with increases in the Ge(II) concentration, but the relationship was not strictly linear. Curve A in Figure 2 shows the latter stage in the reduction of the insoluble polymeric chlorides at potentials more positive than -0.74 V, followed by Ge(II) reduction. Curve B represents a voltammetric scan for which the tungsten microelectrode was not preanodized in the bulk melt. When the scan was first made toward more negative potentials, then reversed, an anodic process began to appear at about -0.75 V, corresponding to the reoxidation of the deposited germanium (Figure 3). This study indicates that constant-potential electrodeposition of germanium should be possible at potentials more negative than -0.8 V.

Chronopotentiometry

In order to observe the behavior of Ge(II) reduction in

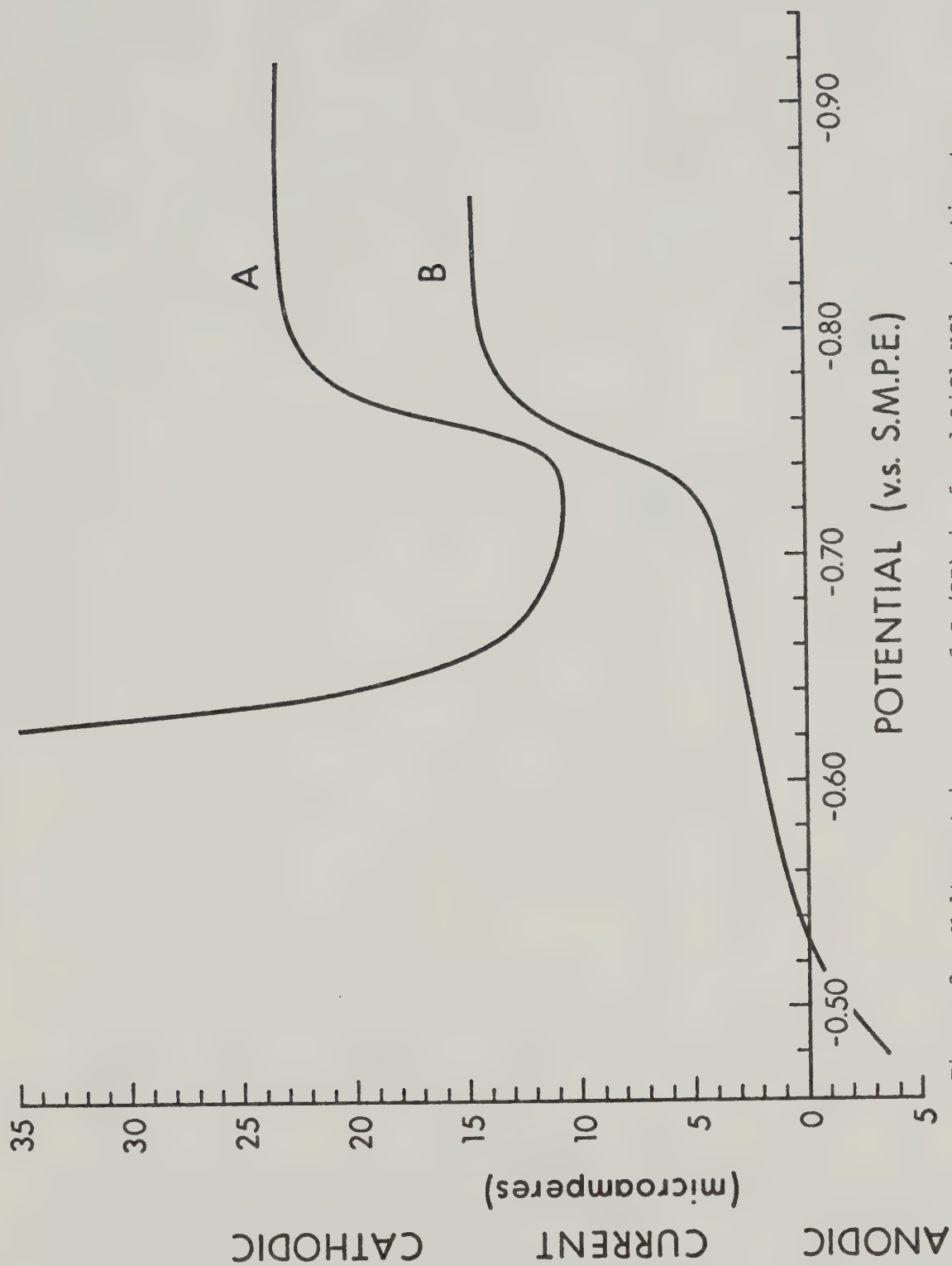


Figure 2. Voltammetric scans of Ge(II) in fused LiCl-KCl eutectic at 450°C, using a tungsten microelectrode. Curve A was obtained with preanodization of the tungsten microelectrode; curve B is a repeated scan with no preanodization.

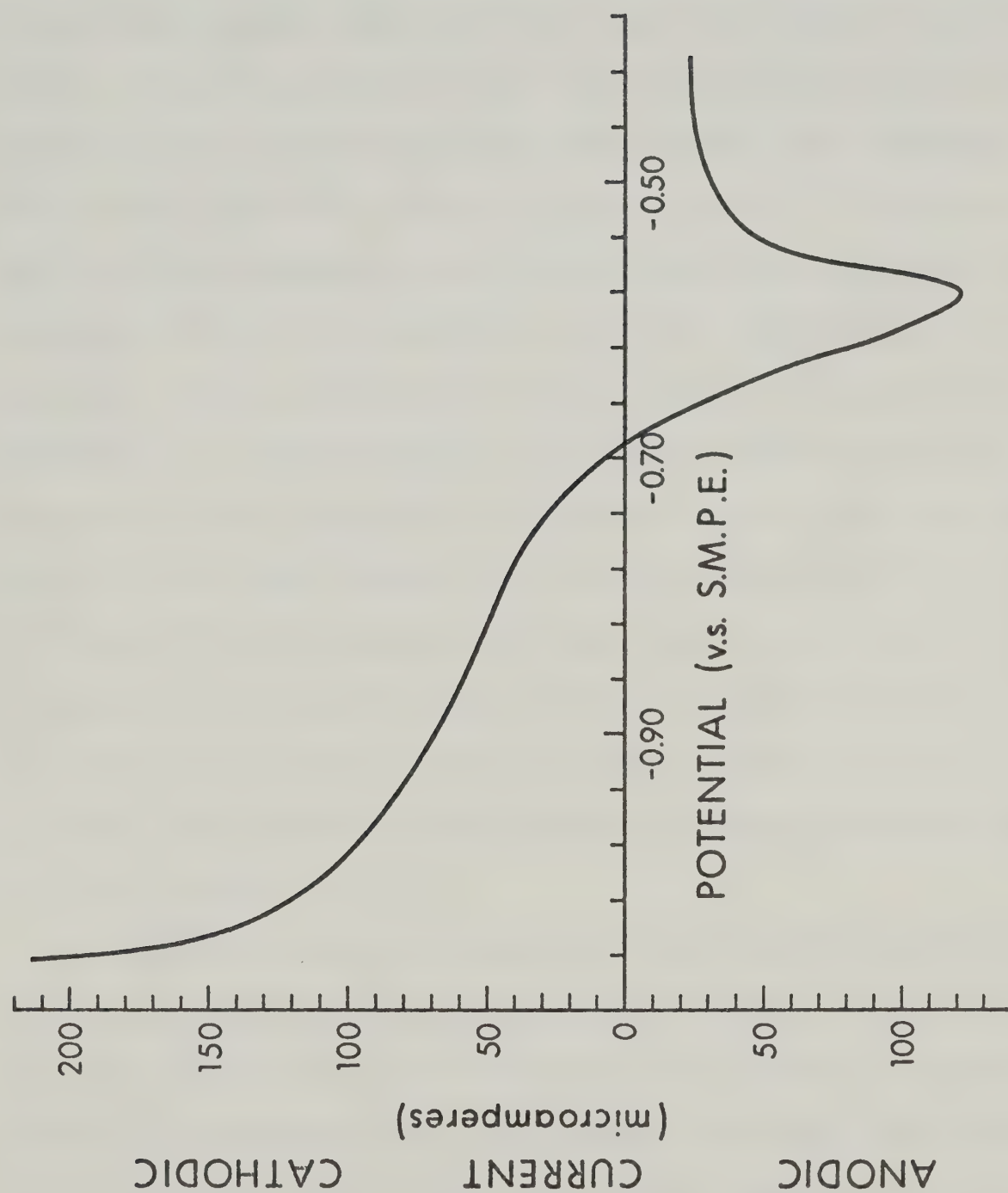


Figure 3. Anodic voltammogram of electrodeposited germanium on a tungsten microelectrode.

the melt under conditions of constant current electrolysis, a chronopotentiometric study was carried out. Chronopotentiometric curves were run at current densities between 12 and 40 mA/cm². A typical curve is shown in Figure 4. The transition region indicated as B was well defined in all cases. The transition(s) at C and beyond were poorly defined at low current densities but became more distinct at current densities greater than 25 mA/cm². The length of the first transition was taken from the origin, A, to B, although an initial dip close to A was observed on all curves. It is believed that this initial dip is due to formation of surface Au-Ge alloy. The transition B is ascribed to the exhaustion of Ge(II) at the electrode surface in the usual manner. The Sand equation, $i\tau^{1/2} = \pi^{1/2} n F A D^{1/2} C/2$, is obeyed for this process as shown in Figure 5, and from the data of Table II the diffusion coefficient of Ge(II) was calculated to be 2.2×10^{-5} cm²/sec, in agreement with values for other divalent ions in this solvent (37).

Using low current densities, and careful observation of the electrode during chronopotentiometry, it was observed that the clean gold electrode took on a bright, mirror-like silver finish soon after the cathodic current flow began. With continued electrolysis the finish continually dulled, until after the end of the first transition, B, when massive black deposits began forming. These deposits, unlike the

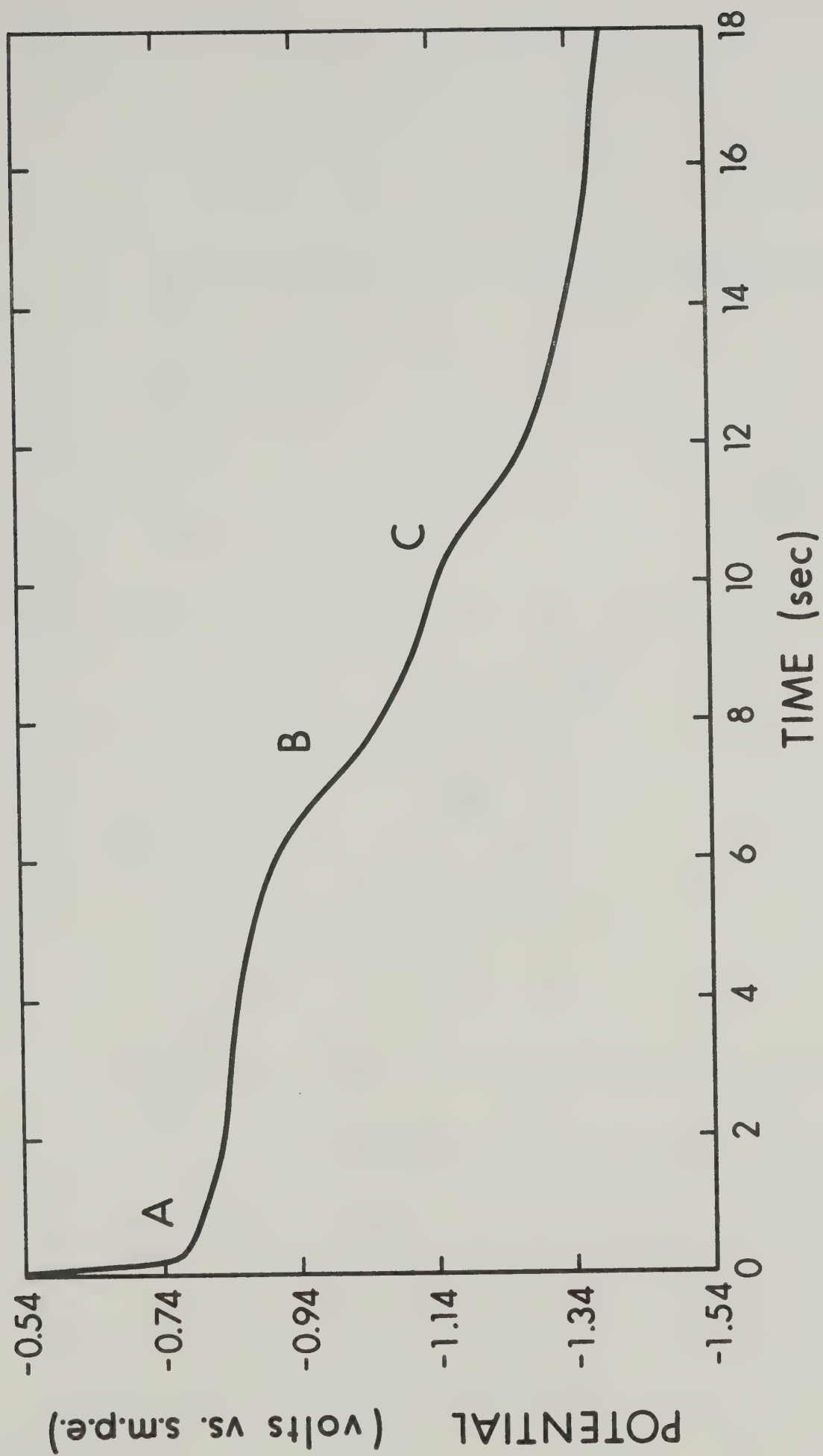


Figure 4. Chronopotentiogram of 1.0×10^{-3} M Ge(II) in the fused LiCl-KCl eutectic at 450°C. Current density was 30 mA/cm².

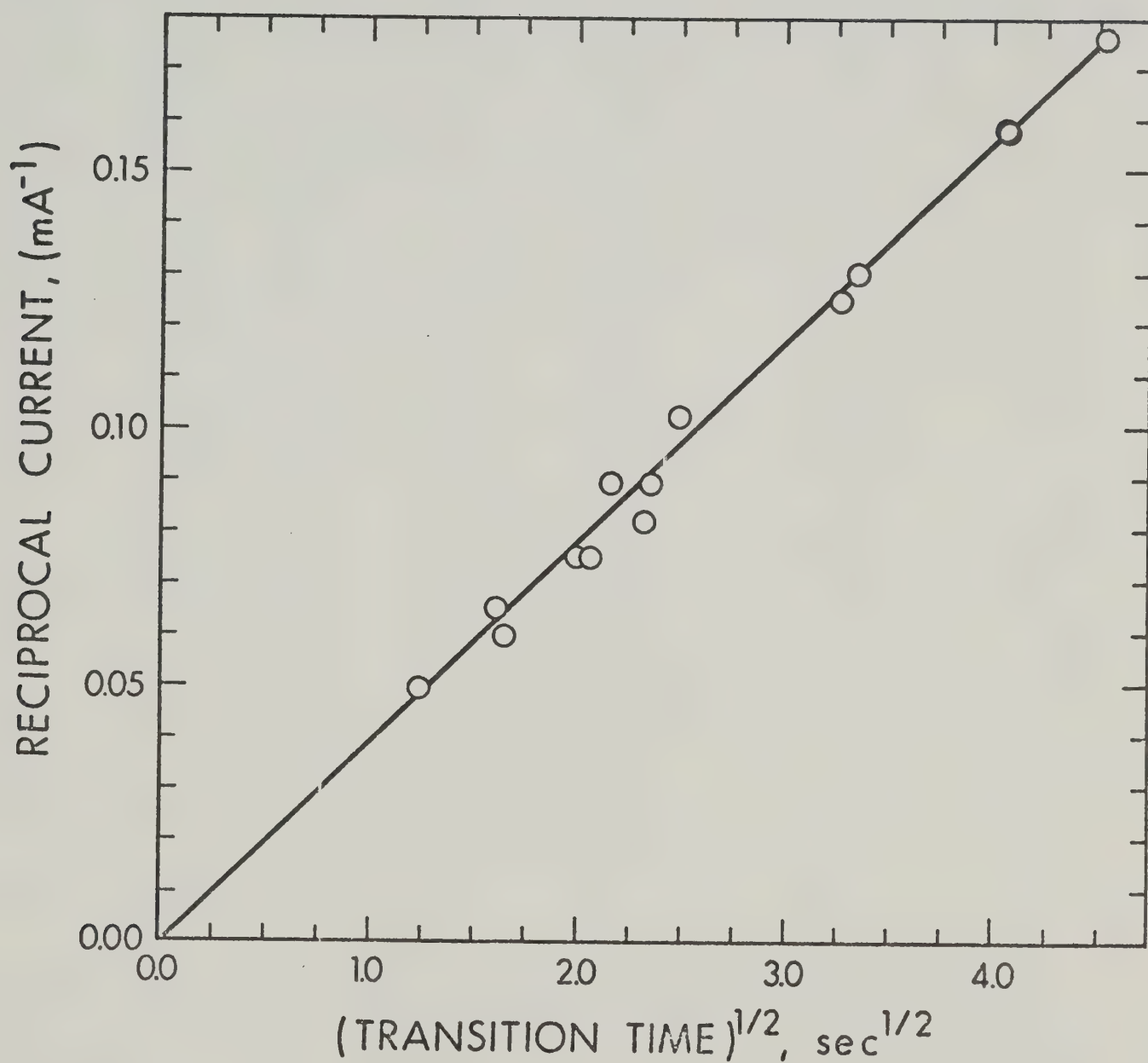


Figure 5. Plot of reciprocal current versus $\tau^{1/2}$ for the first transition in the chronopotentiometric analysis. Concentration of Ge(II), 7.9×10^{-5} mole/cm³; electrode geometric area 0.4 cm².

TABLE II

Chronopotentiometric Data*

Current (mA)	τ_1 (sec)	$i\tau_1^{1/2}$	τ_2 (sec)	$E_{\tau_{1/4}}, V$ (s.m.p.e.)	$E_{\tau_{2/4}}, V$ (s.m.p.e.)	$E_{\tau_{3/4}}, V$ (s.m.p.e.)
5.67	20.5	25.7	—	-0.71	—	—
6.76	16.5	27.5	—	-0.74	—	—
7.70	11.2	25.8	—	-0.72	—	—
7.99	10.7	26.3	—	-0.74	—	—
9.79	6.2	25.5	6.9 [†]	-0.74	—	—
11.15	4.68	24.2	3.8	-0.74	-1.00	-1.2 [†]
11.35	6.00	27.8	5.2	-0.74	-1.06	-1.4 [†]
12.20	5.40	28.4	2.54	-0.77	-1.03	—
13.25	4.23	27.3	7.4 [†]	-0.77	-1.05	-1.2 [†]
13.26	4.35	27.7	3.68	-0.77	-1.04	—
13.31	4.20	26.8	3.0	-0.80	-1.16	-1.4 [†]
15.46	2.50	24.5	3.4	-0.84	-1.14	—
15.72	3.80	30.6	4.5	-0.80	-1.08	-1.3 [†]
16.78 [†]	5.00	27.6	—	-0.81	—	—
20.21 [†]	1.50	24.8	—	—	—	—

* concentration of Ge(II), 7.9×10^{-5} mole/cm³. Electrode geometric area 0.4 cm². $\tau_{1,2,3}$ refer to first, second, and third transition times. Average value of chronopotentiometric constant $i\tau^{1/2}/C$ is $8(\pm 0.5) \times 10^2$ amp sec^{1/2} cm mole⁻¹.

[†] transition ill-defined.

initial finish, did not adhere to the electrode and could be knocked off by gently agitating the gold electrode.

The data for the transitions observed is given in Table II. Measurement of $E_{\tau/4}$ data was difficult due to the fact that not all chlorine generated in the vicinity of the gold electrode could be removed. This led to varying initial values of potentials. To circumvent this problem, the "true" potential of this point was taken from the chronopotentiogram where the lowest current density was used to anodize the germanium from the gold electrode. All potentials were then measured from this point.

At low current densities (less than 17 mA/cm^2) no transition other than the first could be defined. At higher current densities, other transitions became noticeable, especially a well-defined second one. It has been shown by Berzins and Delahay (38) that the Sand equation for a second transition is given by:

$$(\tau_1 + \tau_2)^{1/2} - \tau_1^{1/2} = \pi^{1/2} n_2 F A D_2^{1/2} C_2 / 2i \quad .$$

A plot of $1/i$ versus $(\tau_1 + \tau_2)^{1/2} - \tau_1^{1/2}$ was made for the second transition, but it was found that no linear relation existed. The formation of the black, massive germanium deposit noted at the end of the first transition (B in Figure 4) permits the nonlinearity of the plot of $(\tau_1 + \tau_2)^{1/2} - \tau_1^{1/2}$ versus $1/i$ to be ascribed to the rapidly changing electrode area upon which the

germanium was being deposited. Third transitions were noted at large current densities. These were ill defined, again probably due to rapid electrode area changes.

Thermodynamics of Gold-Germanium Alloy Formation

The gold-germanium phase diagram has been established (34) and shows simple eutectic formation at 12 wt.% germanium. Using this alloy composition, the potential of the cell



was studied over the temperature range from 400°C to 500°C. A preliminary study of the cell showed that Ge(II) is not stable in the LiCl-KCl eutectic melt over extended periods of time when a flow of argon is maintained above the cell assembly; germanium needles grew from the germanium bar and the interior of the upper, cool portion of the apparatus became coated with a white material, presumably GeCl_4 . It was concluded that Ge(II) disproportionates to Ge(IV) and the metal, i.e., $2\text{Ge(II)} \rightleftharpoons \text{Ge(0)} + \text{Ge(IV)}$, where Ge(IV) exists as germanium tetrachloride gas. The equilibrium constant for the disproportionation reaction is $1.69 \times 10^{-2} \text{ l mol}^{-1}$, and thus for a 0.02 M solution of Ge(II), a concentration of Ge(IV) equal to $7 \times 10^{-6} \text{ M}$ is required to maintain equilibrium conditions; however, since Ge(IV) is volatile as $\text{GeCl}_4(\text{g})$, the disproportionation reaction

is slowly forced to the right. To minimize this effect, a static argon atmosphere over the cell was necessary; otherwise, the Ge(II) concentration was reduced to the point where reversible potentials were not obtained.

The temperature-potential measurements of the alloy cell are shown in Figure 6. Data were taken by alternately raising and lowering the temperature; no hysteresis in the cell potential was observed. The cell potential at any given temperature was constant (within 0.1 mV over a 15 min. interval). These facts, together with the observation that the equilibrium cell potential recovered its initial value after passage of small amounts of current in either direction through the cell, showed the system to be reversible. The potential at both the Ge(s) and Au-Ge (12 wt.% Ge, l) electrodes is dictated by the concentration of Ge(II) in solution, since the extent of the reaction $2\text{Au}(0) + \text{Ge}(\text{II}) \longrightarrow \text{Ge}(0) + 2\text{Au}(\text{I})$ is small, as can be seen from the standard potential of the Au(I)/Au(0) couple, +0.205 V (32).

The partial molar entropy of mixing for germanium in the alloy can be determined from the slope of Figure 6 and the relationship $\Delta \bar{S}_{\text{Ge}}^{\text{mix}} = nF(dE/dT)$, where n is the charge on the Ge(II) ion, F is Faraday's constant, and dE/dT is the slope of the potential-temperature plot. The partial molar free energy of mixing for germanium, $\Delta \bar{G}_{\text{Ge}}^{\text{mix}}$, at 450°C is directly calculable from the open circuit potential of the galvanic cell at this temperature.

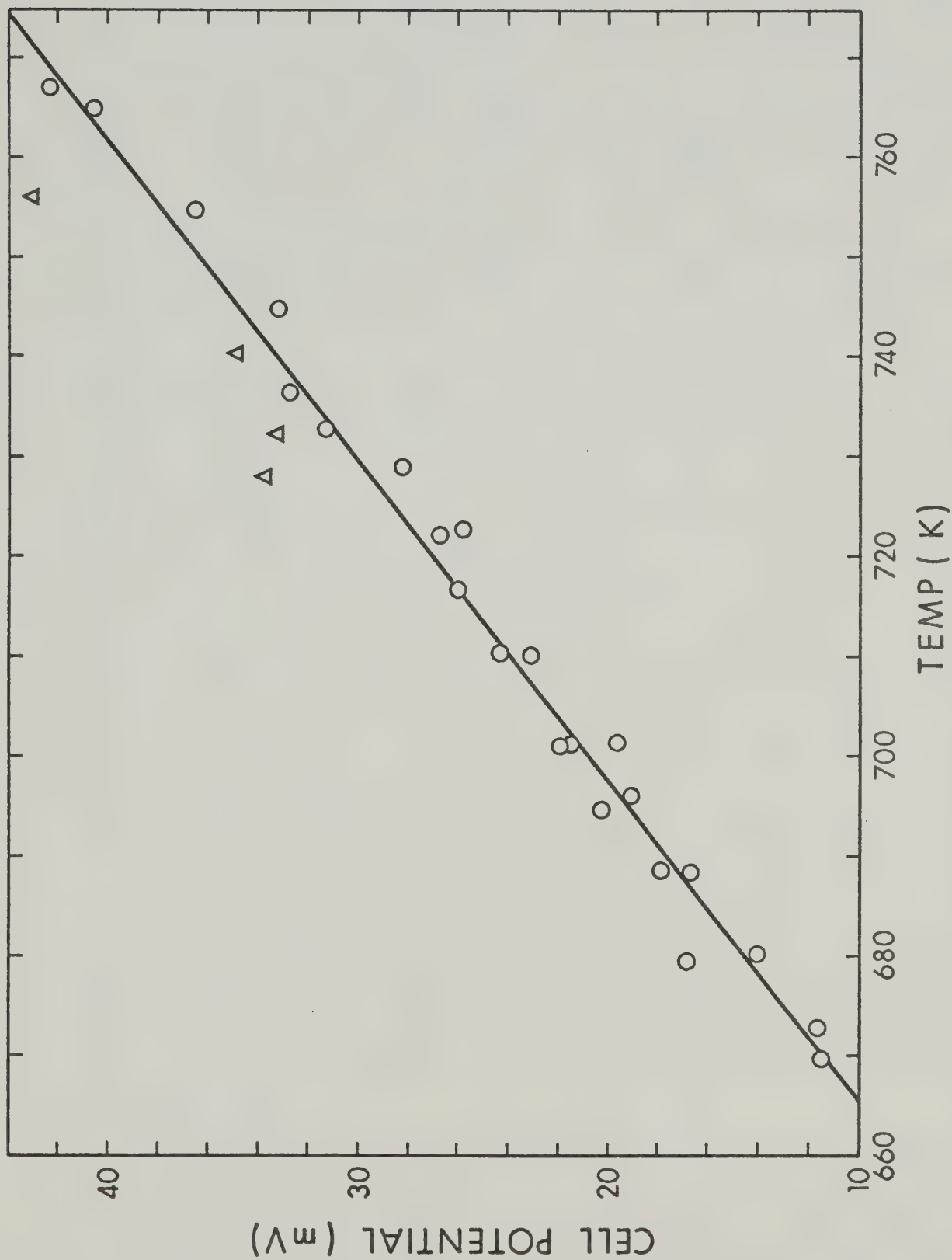


Figure 6. Plot of potential versus temperature for the cell Au-Ge(12 wt. % Ge, l)/Ge(II) in LiCl-KCl/Ge(s). Nonequilibrium values taken in a separate run are indicated by triangles.

The partial molar enthalpy of mixing for germanium, $\Delta \bar{H}_{\text{Ge}}^{\text{mix}}$, is calculable from $\Delta \bar{G}_{\text{Ge}}^{\text{mix}}$ and $\Delta \bar{S}_{\text{Ge}}^{\text{mix}}$. For the alloy Au-Ge (12 wt. % Ge), the following parameters were determined: $\Delta \bar{S}_{\text{Ge}}^{\text{mix}} = 14.2 \pm 0.2$ e.u. ($dE/dT = 3.07 \pm 0.04 \times 10^{-4}$ V/K); $\Delta \bar{G}_{\text{Ge}}^{\text{mix}} = -1.24 \pm 0.02$ kcal/mole; and $\Delta \bar{H}_{\text{Ge}}^{\text{mix}} = +9.00 \pm 0.10$ kcal/mole. By considering the Nernst equations for the half-cells $\text{Ge(II)} + 2e^- \longrightarrow \text{Ge(alloy)}$ and $\text{Ge(0)} \longrightarrow \text{Ge(II)} + 2e^-$, it can be shown that $E_{\text{cell}} = -2.303 \frac{RT}{nF} \log a_{\text{Ge(alloy)}}$, where $E_{\text{cell}} = 26.8 \pm 0.4$ mV at 723 K (after correction for the thermoelectric potential of +9.4 mV between the germanium bar and the tungsten wire used to make contact with the alloy), and $a_{\text{Ge(alloy)}}$ is the activity of germanium in the alloy, which was calculated to be 0.426 ± 0.010 . Defining γ as the activity coefficient of germanium in the alloy and X as the mole fraction of germanium in the alloy, then $a_{\text{Ge(alloy)}} = \gamma X$ (where $X = 0.270$) gives a value of $\gamma = 1.57 \pm 0.03$. Table III gives a comparison of the thermodynamic properties measured in this work with those of other Au-group(IV) element alloys (39,40). It should be noted that the interaction between gold and germanium is small as are the interactions between gold and tin, and gold and lead.

The dip shown at A in Figure 4 corresponds to a shift of approximately 50 mV in potential. The open circuit potential corresponding to the partial molar free energy of mixing for germanium was found to be 26.8 mV. The gold-germanium composition at A is not exactly known, but the

TABLE III

Thermodynamics of Gold-Group IVA-Metal Alloys, 450°C

Metal	Composition, Mole Fraction Metal	$\Delta \bar{G}_{\text{metal}}^{\text{mix}}$ kcal/mole	$\Delta \bar{S}_{\text{metal}}^{\text{mix}}$ e.u.	$\Delta \bar{H}_{\text{metal}}^{\text{mix}}$ kcal/mole	dE/dT, mV/deg	Activity, Metal	Activity Coefficient, Metal
Ge	0.270	-1.24	14.2	+9.00	0.307	0.423	1.57
Sn	0.294	-7.16*	3.66	-4.51*	0.0795	$6.97 \times 10^{-3*}$	0.0237*
Pb	0.270	-2.85*	3.78	-0.12*	0.0820	0.137*	0.507*

* data extrapolated to 450°C

50 mV potential shift at A is of the same order of magnitude as the open circuit potential of the cell at 450°C, and strongly indicates gold-germanium alloy formation.

Using a current density of 50 mA/cm² for approximately 3 seconds, Ge(II) was reduced at the gold electrode and this plate was then anodized. The $E_{\tau/4}$ for the anodic chronopotentiogram (Figure 7) was -0.46 V as compared to $E_{\tau/4}$ for the reduction chronopotentiogram which was of the order of -0.84 V. The potential of the anodic chronopotentiogram did not rise sharply, i.e., oxidation of germanium was extended over a large period of time. This behavior is also indicative of alloy formation. The dashed line AB (Figure 7) is the behavior expected for the oxidation of germanium in the absence of alloy formation. The wavy nature of the chronopotentiogram (Figure 7) is due to chlorine evolution.

Topography of Germanium Deposited onto Gold

A. Optical Metallography

Micrograph 1 is a cross-sectional view of germanium deposited onto gold, as previously described. The middle band, which appears most heavily scratched, is the gold substrate; it was found to have an average width of 160 μm . Since the original width of the gold flag was 250 μm , there was considerable reduction (90 μm or 35%) in the

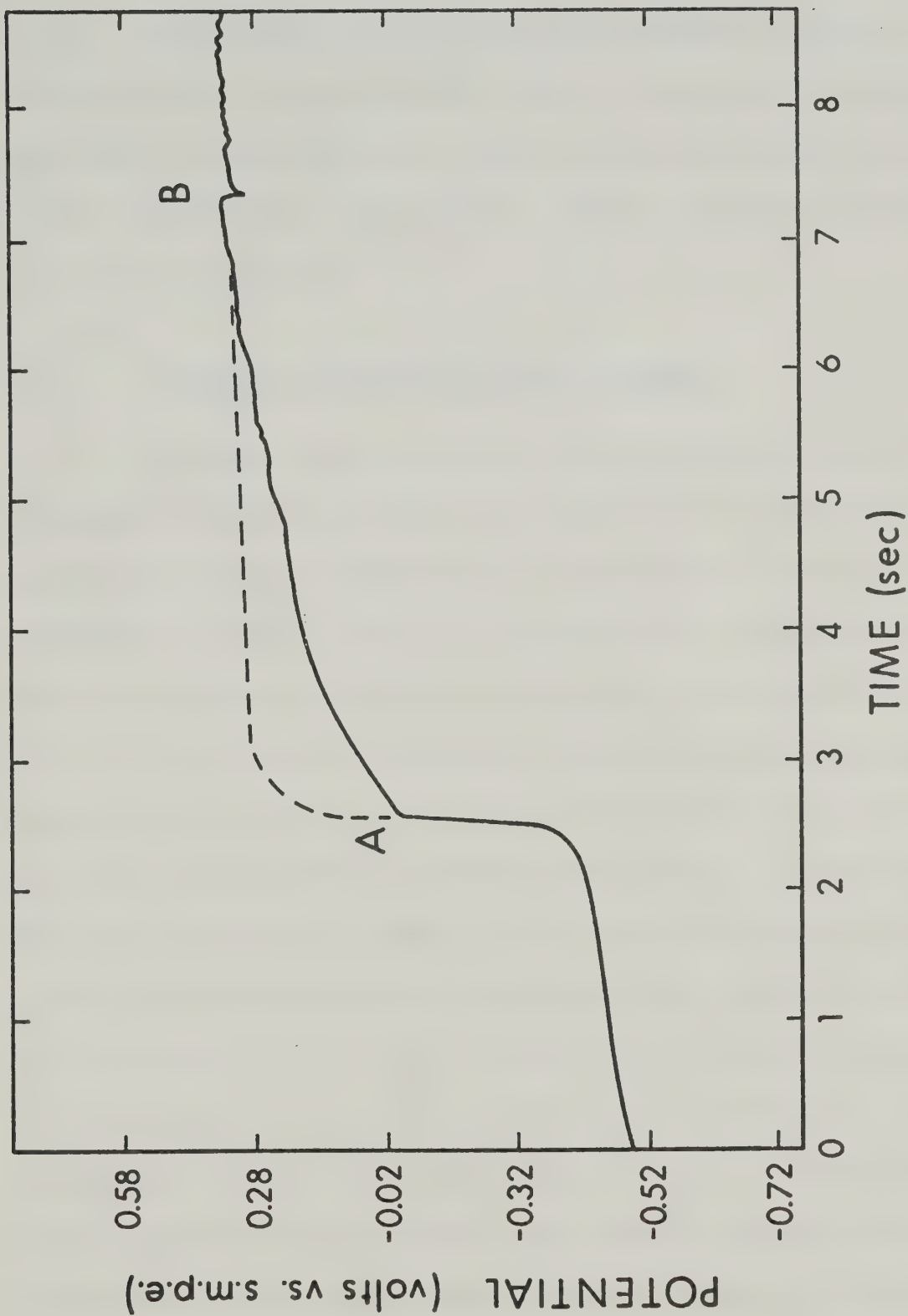


Figure 7. Anodic chronopotentiogram of germanium on a gold flag (0.4 cm² in area). Ge(II) was reduced onto the gold using a 10 mA current for 10 seconds. Anodizing current was 20.0 mA.

width of the gold. The outer layers were found to have a total width of 340 μm , and are not pure germanium. They most resemble the gold-germanium eutectic, which can be discerned by its structure (41). In several regions the germanium penetrated the gold band, in tracks, so that both outer layers were connected. These tracks had a blue-grey coloration to them.

B. Scanning Electron Metallography

Several reviews have been published describing the scanning electron microscope (42,43,44). Basically, the scanning electron microscope operates as follows. A hot tungsten filament acts as a source of a thermionically emitted electron beam whose diameter is reduced from 50 μm to 10 nm by magnetic lenses. The resulting electron beam represents a very small probe, and a large depth of field of view can be attained with this probe. Between the magnetic reduction lenses is an electrostatic or magnetic field which deflects the electron beam in both horizontal and vertical directions so that the electron probe scans the surface of the specimen in a raster fashion. Secondary electrons emitted from the sample are collected, amplified, and displayed on a cathode ray tube in synchronism with the scanning electron beam. The net result of this process is to create the exact image of the specimen on the cathode ray tube that was scanned by the electron probe. Image con-

trast results from signal variations in the number of secondary electrons produced.

Electron micrographs obtained on a scanning electron microscope have a three-dimensional appearance. This may be fully exploited by obtaining a stereographic view of the surface, which is accomplished by taking two exposures of the specimen and altering the angle of the specimen with respect to the electron probe between exposures. When the two micrographs are combined, by observing the pair through a stereoscope, a stereographic view is obtained. The magnification which can be achieved with the scanning electron microscope ranges from 20 X to 100,000 X, and the microscope has a resolution of about 100 \AA .

Scanning electron micrographs were taken of numerous samples of germanium deposited onto gold. The samples were obtained either by allowing the sample to slowly cool in the LiCl-KCl eutectic melt as the melt froze, or by withdrawing the sample from the eutectic melt and rapidly cooling it to room temperature. Needle-like deposits, composed of germanium, were noted in all experiments utilizing constant potential as the mode of electrodepositing germanium. These needles varied up to 1 cm in length and up to 200 μm in width, and grew from the gold-germanium interface into the solution. A scanning electron micrograph of a typical needle is shown in Micrograph 2.

1. Micrographs after First Transition Time - Sample
Rapidly Cooled.

To the naked eye, the surface had a bright, silvery appearance. The germanium deposit did not completely coat the gold surface, as small regions of the gold underlay were readily visible. A micrograph at a magnification of 100 X confirmed this visual observation, and showed the germanium deposit to be smooth. At a magnification of 1000 X, Micrograph 3, the streaked gold underlay is clearly visible; the germanium deposit about the underlay rises to a ridge before forming the bulk deposit.

2. Micrograph after Second Transition Time - Sample
Rapidly Cooled.

Visual examination of the sample showed the deposit to be silver-like in color with most of the gold underlay being covered. The germanium deposit covered more of the gold underlay in this sample than in the previous one. This is to be expected, as more current is passed in going to the second transition than is passed in going to the first transition. At a magnification of 5000 X, Micrograph 4, the surface shows a veined structure, and portions of the gold underlay are discernible.

3. Micrograph of the Surface after Flash Constant
Potential Electrolysis of Ge(II) - Sample Rapidly
Cooled.

This sample was prepared by applying a constant potential of -0.85 V to the gold flag for a period of no longer than 10 seconds. The deposit was bright silver in color, and covered all of the gold surface. Total surface coverage is not surprising because of the large initial current obtained when a constant reducing potential is applied to the working electrode. A micrograph at a magnification of 10,000 X, Micrograph 5 shows the surface to be extremely smooth.

4. Micrographs of the Surface after Extended Constant Potential Electrolysis of Ge(II) - Sample Rapidly Cooled.

The gold foil electrode was electrolyzed at a constant potential of -0.85 V over a period of 20 hours in a solution which was originally 0.2 M in Ge(II). A massive group of germanium needles were found adhering to the gold electrode at the end of the electrolysis period.

At a magnification of 2000 X, Micrograph 6, a stereographic pair, shows a predominantly smooth, striated underlay over which appears a rosette formation. In some areas, "bubbles" are found together with the rosettes. The rosettes may be regions where germanium needles broke off from the surface deposit, or may be indicative of gold-germanium alloy formation. In certain regions, the striations do not run in one direction, but appear to change

directions. Where this occurs, a V-like pattern is formed. This is shown at a magnification of 2000 X in Micrograph 7, which is also a stereographic pair. A region of the striated surface was found where thermal cracking occurred as a result of the rapid sample cooling. Micrograph 8 (5000 X) depicts this feature and shows the deposit to be layered. The cracks are at least 3 μm deep.

5. Micrograph of the Surface after Extended Constant Potential Electrolysis of Ge(II) - Sample Slowly Cooled.

The deposition of germanium took place as described for the previous sample. To the naked eye, the sample looked much like brass, and its surface was rough in appearance. Micrograph 9, at a magnification of 1000 X, shows the surface to be veined and cluttered with "debris", the debris most likely being particles of germanium.

6. Micrograph of the Surface after Extended Constant Potential Electrolysis of Ge(II) - Sample Slowly Cooled.

The deposition potential employed for the production of this sample was -0.80 V. Again, the initial concentration of Ge(II) was 0.2 M. The deposit was aluminum-colored, and contained regions where the gold underlay was visible. No large germanium needles were produced, but the black, bulky, nonadherent deposit evident in all electrolyses (except

for the constant current electrolysis of Ge(II) to the first transition) was noted. The sample had a dull finish, and was fairly smooth in appearance. The topography of this sample, as shown in Micrograph 10 at a magnification of 5000 X, depicts flat-topped, steeply rising protrusions that are joined to one another.

7. General Remarks

Rapidly cooled samples of germanium deposited onto gold gave rise to smoother surfaces than did the samples which were slowly cooled. This is not surprising, since rapid cooling of the sample to room temperature will tend to retain the composition of the alloy as it was at 450°C, and hence, retain most of the surface features of the alloy at that temperature. (All deposits of germanium on gold in the melt at 450°C had a smooth appearance). Slow cooling of the sample from 450°C to room temperature allows gold and germanium to separate as dictated by the phase diagram of this system; hence, a rougher surface is produced by slow sample cooling.

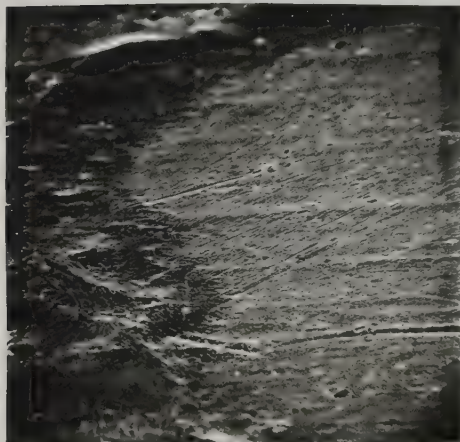
Use of large current densities, i.e., use of more negative reduction potentials in the reduction of an electroactive species from solution generally leads to a rough surface formation, while use of small current densities, i.e., use of more positive reduction potentials leads to a more uniform surface formation. Thus, the topography



Metallograph 1.



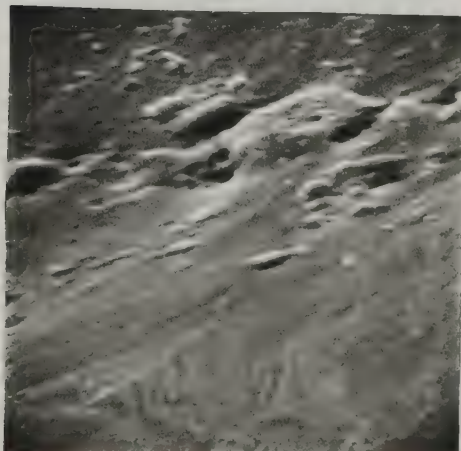
50μm Metallograph 2.



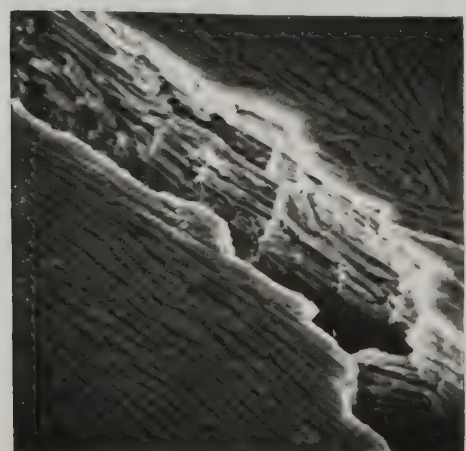
10μm Metallograph 3.



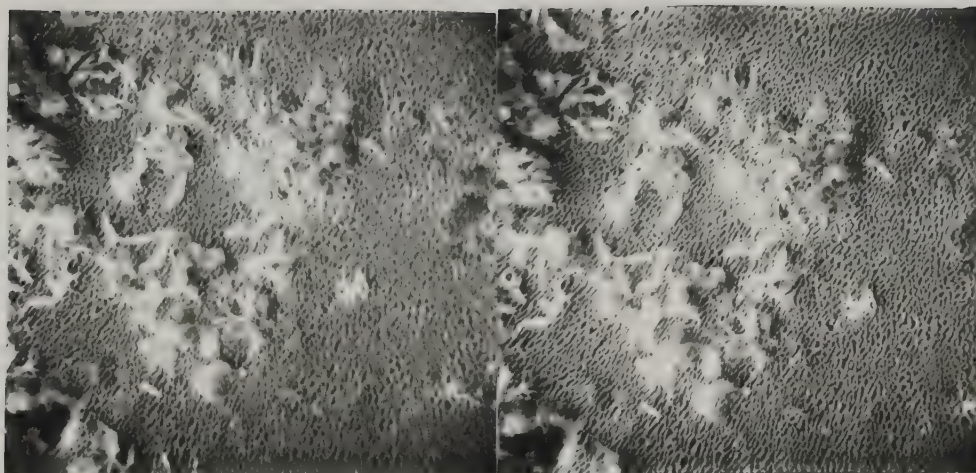
2μm Metallograph 4.



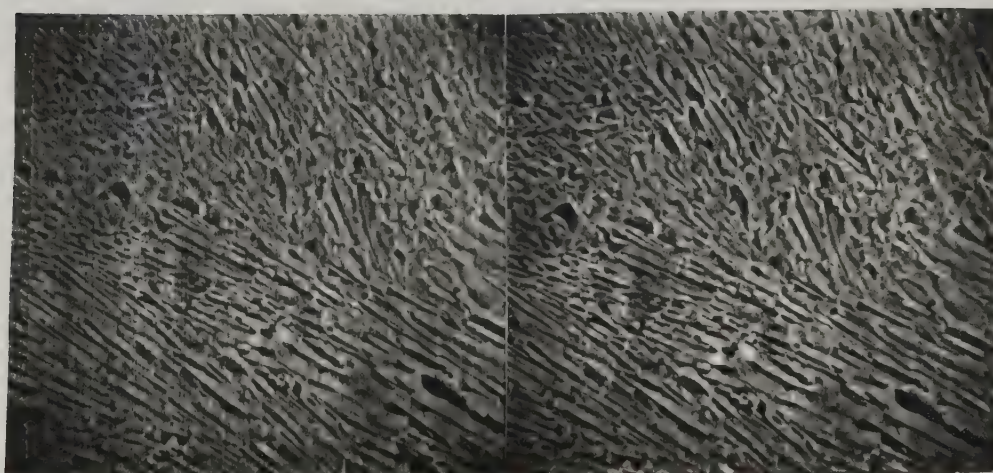
1μm Metallograph 5.



2μm Metallograph 8.



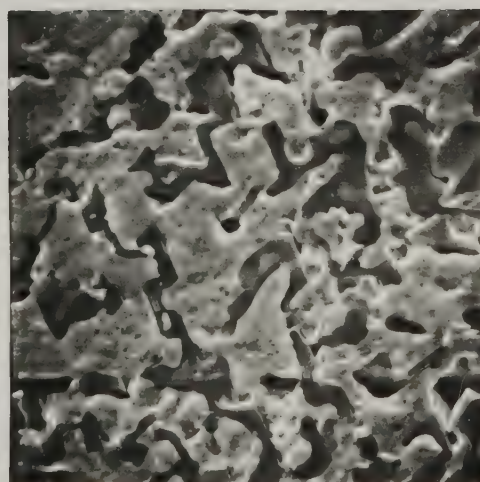
5 μ m Metallograph 6.



5 μ m Metallograph 7.



10 μ m Metallograph 9.



5 μ m Metallograph 10.



of the sample obtained by reduction of Ge(II) at -0.85 V was much rougher than that of the sample obtained by reduction of Ge(II) at -0.80 V (see parts 5 and 6 above).

Tin

A liquid tin pool was anodized to prepare a solution of Sn(II) for use in the determination of the standard potential of the Sn(IV)/Sn(II) redox couple. In the course of this anodization, eight concentration-potential data points were collected so that a comparison of the value of the Sn(II)/Sn(0) standard potential could be made against the value obtained by Laitinen and Liu (32), who electrolytically reduced Sn(II) (added to the melt as anhydrous tin(II) chloride) in stages to obtain concentration-potential data. The current density employed in the anodization of the tin pool was approximately 40 mA/cm^2 . The concentration of Sn(II) ranged from 1.68×10^{-2} to 0.194 M . A plot of $\log [\text{Sn(II)}]$ as a function of the cell potential was linear and had a slope of $0.071 \pm 0.002 \text{ V/log unit}$, in agreement with the theoretical value of 0.072 V/log unit for a two-electron process at 450°C . The standard potential determined for the Sn(II)/Sn(0) couple was -1.079 V , with a standard deviation of less than 1 mV . This value, corrected for the thermoelectric potential between platinum and tungsten, compares favorably with the value of $-1.082 \pm 0.002 \text{ V}$ obtained by Laitinen and Liu (32).

The Sn(II) solution was further oxidized to Sn(IV) at a graphite electrode after the tin electrode had been removed from its isolation compartment. The current density employed for this process was approximately 0.6 mA/cm^2 . Few points could be taken in any one experiment because, as the anodization of Sn(II) proceeded, the polarization potential of the graphite anode steadily drifted to more positive values. In order to maintain the polarization potential below chlorine evolution ($\sim +0.3 \text{ V}$), the experiment had to be interrupted repeatedly, whereupon the graphite anode was shaken in the melt. This alleviated the problem somewhat, but did not completely eliminate it, as the amount of current which could be passed between interruptions became progressively smaller; eventually it became impractical to continue the experiment. Careful observation of the graphite electrode did not reveal tin tetrachloride gas evolution. Agitation of the graphite electrode during electrolysis did not reduce the increasing polarization potential, and hence this phenomenon cannot be attributed solely to concentration polarization of the graphite anode, i.e., to the depletion of Sn(II) at the surface of the graphite electrode. Although the polarization potential increased during the oxidation of Sn(II), it did not stop at chlorine evolution, but went several hundred mV beyond that potential. Normally, anodization of a graphite electrode in the fused LiCl-KCl eutectic results

in chlorine evolution, and at low current densities this process occurs at a constant potential of about +0.3 V. These observations can be explained on the basis that the tin tetrachloride gas formed in the anodization of Sn(II) is adsorbed onto or into the graphite electrode; it is nonconductive, so that a greater potential is required to pass current through the graphite anode. After current cessation, stirring of the solution with the graphite anode resulted in the return of its potential to a steady value well within the potential range of the melt. The tin tetrachloride gas adsorbed onto or into the graphite anode during Sn(II) oxidation must dissolve in the melt during this time. Fourteen data points were thus collected in three separate experiments; the concentration ratio of Sn(II) to Sn(IV) varied from 6.86 to 3.58. A plot of $\log [\text{Sn(II)}]/[\text{Sn(IV)}]$ as a function of the observed cell potential was linear, and had a slope of 0.063 ± 0.005 V/log unit, in fair agreement with the theoretical value of 0.072 V/log unit for a two-electron process at 450°C. It is not surprising that the value of the slope obtained in the Nernst plot is low, as Sn(IV) volatilized slowly from solution as $\text{SnCl}_4(\text{g})$. This was evidenced by the slight presence of white fumes when the tin compartment was exposed to the atmosphere at the end of the experiment. (Delarue (4) has reported the volatility of tin tetrachloride from the LiCl-KCl eutectic melt. He oxidized Sn(II) with Cu(II) and noted the evolution

of tin tetrachloride gas). Loss of Sn(IV) by volatilization of $\text{SnCl}_4(\text{g})$ was not serious, as the potential of the graphite electrode remained constant (maximum drift was 4 mV in 30 minutes) after cessation of Sn(IV) generation and stirring. The standard state of Sn(IV) was taken as unit concentration of Sn(IV) in solution. The standard potential of the Sn(IV)/Sn(II) redox couple was determined to be -0.310 ± 0.003 V; this value has been corrected for the thermoelectric potential of +0.004 V between platinum and graphite at 450°C. In view of the adsorption of $\text{SnCl}_4(\text{g})$ onto the graphite electrode, and the possibility that not all $\text{SnCl}_4(\text{g})$ was desorbed, the standard deviation of ± 0.003 V must be taken to represent the lower limit of uncertainty in the standard potential of the Sn(IV)/Sn(II) couple.

Delarue (4) carried out a voltammetric study of the oxidation of Sn(II) at a graphite electrode in the LiCl-KCl eutectic melt, and reported the half-wave potential for the oxidation of Sn(II) to Sn(IV) to be 0.0 V. This value is reasonable, since Delarue (4) has shown that Cu(II) will oxidize Sn(II) to Sn(IV); therefore, the standard potential - which is approximately equal to the half-wave potential of a voltammetric curve - of the Sn(IV)/Sn(II) couple must be less than +0.061 V, the standard potential of the Cu(II)/Cu(I) couple (32). However, the value of the half-wave potential determined by Delarue (4) did not correspond to the standard potential of the

Sn(IV)/Sn(II) couple determined in this work, and the voltammetric study was therefore repeated. A graphite rod, sharpened to a point and dipping into the melt a distance of 1-2 mm, was used as the indicating electrode. Scanning anodically, only one wave was observed, and the half-wave potential of this wave was found to be -0.31 V, in excellent agreement with the standard potential of the Sn(IV)/Sn(II) redox couple determined in this study. Reduction of Sn(II) at the graphite microelectrode gave rise to large, ill-defined waves as expected, due to the large concentration of Sn(II) present. The voltammetric wave crossed the zero current axis at -1.1 V, in agreement with the standard potential of the Sn(II)/Sn(0) couple. The difference between Delarue's value (4) of the half-wave potential for the oxidation of Sn(II) to Sn(IV) and that obtained in this study can be explained as follows. Delarue employed larger current densities and longer electrolysis times to obtain voltammetric data in the oxidation of Sn(II) to Sn(IV) (33). This would have resulted in the adsorption of $\text{SnCl}_4(\text{g})$ onto the electrode, thereby causing a significant shift of the half-wave potential in the positive direction. Also, Delarue (4) did not purify his melt, nor was his cell kept under an inert atmosphere, so contamination of the melt by traces of water and oxygen may account for all or part of the discrepancy.

Reversibility of the Sn(IV)/Sn(II) couple was

determined by a micropolarization technique. Small amounts of current were passed in either direction through the graphite electrode, and it was observed that the open circuit potential of the cell recovered its initial value within 30 seconds of current cessation.

From the standard potentials of the Sn(II)/Sn(0) and Sn(IV)/Sn(II) couples, the standard potential of the Sn(IV)/Sn(0) couple was calculated to be -0.694 ± 0.003 V, and the equilibrium constant for the reaction $2\text{Sn(II)} \rightleftharpoons \text{Sn(0)} + \text{Sn(IV)}$ was calculated to be $1.88 \times 10^{-11} \text{ l mol}^{-1}$. Thus Sn(0) and Sn(IV) will react quantitatively to produce Sn(II) . The standard potentials of tin are reported on the molar, molal, and mole fraction scales in Table IV, p.109, and the equilibrium constants for the disproportionation of the other divalent group IVA cations are given in Table V, p.111.

Lead

In an attempt to determine the standard potential of the Pb(IV)/Pb(II) redox couple, a lead pool was coulometrically oxidized to initially produce a solution of Pb(II) . Ten concentration-potential data points were collected during this anodization so that the value of the standard potential of the Pb(II)/Pb(0) couple could be determined and compared with that calculated by Laitinen and Liu (32), who, as in the determination of the standard potential of the Sn(II)/Sn(0) couple, obtained concentration-potential data

by coulometric reduction of Pb(II) which had been added to the eutectic melt as anhydrous lead(II) chloride. The current density employed in the oxidation of the lead pool was approximately 40 mA/cm^2 , and the concentration of Pb(II) varied from 2.00×10^{-2} to 0.126 M . A plot of $\log [\text{Pb(II)}]$ against the observed cell potential was linear, and had a slope of $0.072 \pm 0.002 \text{ V/log unit}$, in agreement with the theoretical value of 0.072 V/log unit for a two-electron process at 450°C . The standard potential calculated for the Pb(II)/Pb(0) couple, corrected for the thermoelectric potential of $+0.005 \text{ V}$ between platinum and tungsten, was $-1.093 \pm 0.002 \text{ V}$, which is in agreement with the value of $-1.101 \pm 0.002 \text{ V}$ obtained by Laitinen and Liu (32) for the same system.

Attempts to further oxidize Pb(II) at a graphite electrode (current density employed was approximately 0.6 mA/cm^2) resulted only in chlorine evolution. This means that Pb(II) is the highest oxidation state of lead obtainable in the fused LiCl-KCl eutectic (in accordance with Delarue's study (4) of lead oxides in this melt), and that the standard potential of the Pb(IV)/Pb(II) redox couple must be greater than the standard potential of the $\text{Cl}_2(\text{g})/\text{Cl}^-$ couple, $+0.322 \text{ V}$, which was determined by Laitinen and Pankey (45). From the value of the standard potential of the Pb(II)/Pb(0) couple determined in this study, and the knowledge that the standard potential of the

Pb(IV)/Pb(II) couple must be greater than +0.322 V, it can be shown that the standard potential of the Pb(IV)/Pb(0) redox couple must be more positive than -0.386 V, and that the value of the equilibrium constant for the reaction $2\text{Pb(II)} \rightleftharpoons \text{Pb(0)} + \text{Pb(IV)}$ must be less than $2 \times 10^{-20} \text{ l mol}^{-1}$.

Discussion of Standard Potentials

Table IV, p.109, summarizes the standard potentials of the group IVA elements on the molar, molal, and mole fraction scales. Two limiting cases were encountered in the determination of the standard potentials of the Ge(IV)/Ge(II) and Sn(IV)/Sn(II) couples. The first case corresponds to the situation where both forms of the redox couple are soluble in the eutectic melt. The other case corresponds to the situation where the reduced form of the redox couple is soluble in the melt, but the oxidized form volatilizes from it. Although tin tetrachloride is somewhat volatile from the fused LiCl-KCl eutectic, it was not generated in large enough quantities in this work to significantly volatilize from the melt, and therefore the Sn(IV)/Sn(II) couple represents the first case. The Nernst equation for this system is:

$$E = E^{\circ'} + 0.0717 \log \frac{[\text{Sn(IV)}]}{[\text{Sn(II)}]} + 0.0717 \log \frac{\gamma_{\text{Sn(IV)}}}{\gamma_{\text{Sn(II)}}} .$$

TABLE IV

Standard Potentials of the Group IVA Elements inLiCl-KCl Eutectic, 450°C

<u>System</u>	<u>E°_{molar}</u>	<u>E°_{molal}</u>	<u>E°_X</u>	<u>Standard Deviation</u>
C	>+0.322	>+0.306	>+0.216	-
Si	-	-	-	no rev. pot.
Ge (II) / Ge (0)	-0.792	-0.792	-0.792	0.008
Sn (II) / Sn (0)	-1.079	-1.079	-1.079	<0.001
Sn (II) / Sn (0) [†]	-1.082	-1.082	-1.082	0.002
Pb (II) / Pb (0)	-1.093	-1.093	-1.093	0.002
Pb (II) / Pb (0) [†]	-1.101	-1.101	-1.101	0.002
Ge (IV) / Ge (II)	-0.665	-0.681	-0.771	0.002
Sn (IV) / Sn (II)	-0.310	-0.326	-0.416	0.003
Pb (IV) / Pb (II)	>+0.322	>+0.338	>+0.428	not measurable
Ge (IV) / Ge (0) *	-0.728	-0.736	-0.781	0.008
Sn (IV) / Sn (0) *	-0.694	-0.702	-0.747	0.003
Pb (IV) / Pb (0) *	>-0.386	>-0.394	>-0.439	estimate

[†] Reference 29.

* Calculated from experimental free energies determined in this work.

Since plots of E as a function of $\log \text{Sn(IV)}/\text{Sn(II)}$ were linear, the above equation can be re-written as:

$$E = E^\circ + 0.0717 \log \frac{[\text{Sn(IV)}]}{[\text{Sn(II)}]} .$$

This latter form of the Nernst equation was used to determine the standard potential of the $\text{Sn(IV)}/\text{Sn(II)}$ couple. The standard state of Sn(IV) and of Sn(II) was taken as unit concentration of the species in solution.

The $\text{Ge(IV)}/\text{Ge(II)}$ redox system represents the other limiting case, i.e., the situation where the oxidized form of the redox couple volatilizes from the melt. As previously derived, the Nernst equation employed in the determination of the standard potential of the $\text{Ge(IV)}/\text{Ge(II)}$ couple was

$$E = E^\circ - 0.0717 \log [\text{Ge(II)}] + 0.0717 \log a_{\text{Ge(IV)g}} .$$

In using this expression, a different definition of the standard state of a gas was employed, namely that the activity of germanium tetrachloride gas produced throughout the anodization of Ge(II) is unity. The standard state of a gas is normally defined as the pure gas at one atmosphere pressure at the operating temperature of the system. Under the conditions of these experiments, germanium tetrachloride gas volatilized from solution as it was produced, and hence, was not present at one atmosphere pressure during the measurement of the cell

potential. However, if the activity of the germanium tetrachloride gas was only one-tenth of its defined value (unit activity) during measurement of the cell potential, a change of -0.072 V in the standard potential of the Ge(IV)/Ge(II) redox couple would occur, and this would not alter the overall trend of the M(IV)/M(II) standard potentials.

Stability of the M(II) Oxidation State

Table V below summarizes the values of the equilibrium constants for the reaction $2\text{M(II)} \rightleftharpoons \text{M(0)} + \text{M(IV)}$:

TABLE V

Stability of the M(II) Oxidation State of the Group IVA
Elements in LiCl-KCl Eutectic at 450°C

<u>Reaction</u>	<u>Equilibrium Constant (1 mol^{-1})</u>
$2\text{Ge(II)} \rightleftharpoons \text{Ge(0)} + \text{Ge(IV)}$	1.69×10^{-2}
$2\text{Sn(II)} \rightleftharpoons \text{Sn(0)} + \text{Sn(IV)}$	1.88×10^{-11}
$2\text{Pb(II)} \rightleftharpoons \text{Pb(0)} + \text{Pb(IV)}$	$<2 \times 10^{-20}$

From this table, it can be seen that the order of ion stability is $\text{Pb(II)} > \text{Sn(II)} > \text{Ge(II)}$. It is thermodynamically unfavorable for Ge(II) to completely disproportionate, but the reaction is forced to completion by the volatility of Ge(IV) (germanium tetrachloride gas) at 450°C. Tin(II) and

Pb(II) are very stable in the melt, and show no tendency to disproportionate. The inability to coulometrically oxidize Pb(II) to a higher oxidation state exemplifies its stability in the eutectic melt.

C O N C L U S I O N

Carbon, silicon, and silicon tetrachloride are electrochemically inactive in the fused LiCl-KCl eutectic. The M(II) oxidation state becomes more stable in going from germanium to lead. Germanium and tin exist in the M(0), M(II), and M(IV) oxidation states, while lead only exists as Pb(0) and Pb(II) in the melt. The standard reduction potentials between different oxidation states of the same element have been determined. Germanium metal can be electrodeposited from this melt; the reduction process on gold is complicated by alloy formation. A thermodynamic study of gold-germanium eutectic-alloy formation has shown that the interaction between gold and germanium in the alloy is small. A morphological examination of germanium deposited onto gold has shown that the topography of the deposit varies according to the conditions employed to plate germanium.

B I B L I O G R A P H Y

1. D. R. Morris and J. R. Harry, Proc. Intern. Conf. Industrial Carbon and Graphite. Soc. Chem. Ind. London. 1965. pp.36-47.
2. J. A. Plambeck, unpublished work.
3. R. Barde, R. Buvet, and J. Dubois, C. R. Acad. Sci., Paris, Ser. C, 225, 1627 (1962).
4. G. Delarue, J. Electroanal. Chem., 1, 285 (1959).
5. K. Arndt and H. Probst, Z. Elektrochem., 29, 323 (1923).
6. C. S. Taylor, Trans. Electrochem. Soc., 27, 301 (1925).
7. R. E. Panzer, Electrochem. Technol., 2, 10 (1964).
8. C. Winkler, J. prakt. Chem., 34, 208 (1886).
9. U. C. Tainton and E. T. Clayton, Trans. Electrochem. Soc., 57, 279 (1930).
10. J. I. Hall and A. E. Koenig, Trans. Electrochem. Soc., 65, 215 (1934).
11. R. Schwarz, F. Heinrich, and E. Hollstein, Z. anorg. allgem. Chem., 229, 146 (1936).
12. C. G. Fink and V. M. Dokras, J. Electrochem. Soc., 95, 80 (1949).
13. J. E. Land, J. Alabama Acad. Sci., 20, 37 (1948).
14. F. Jirsa, Z. anorg. allgem. Chem., 268, 84 (1952).
15. M. V. Sullivan, D. L. Klein, R. M. Finne, L. A. Pompliano and G. A. Kolb, J. Electrochem. Soc., 110, 412 (1963).

16. W. E. Reid, Jr., J. Phys. Chem., 69, 3168 (1965).
17. M. L. Nichols and S. R. Cooper, Ind. Eng. Chem., Anal. Ed., 7, 350 (1935).
18. B. Lovrecek and J. O'M. Bockris, J. Phys. Chem., 63, 1368 (1959).
19. G. Szekely, J. Electrochem. Soc., 98, 318 (1951).
20. K. M. Tressler and L. M. Dennis, J. Phys. Chem., 31, 1429 (1927).
21. C. G. Fink and C. C. Ma, Trans. Electrochem. Soc., 84, 33 (1943).
22. M. J. Barbier-Andrieux, Ann. chim. (Paris), 10, 754 (1954).
23. J. L. Andrieux and M. J. Barbier-Andrieux, C. R. Acad. Sci., Paris, 240, 2104 (1955).
24. J. O'M. Bockris, J. Diaz, and M. Green, Electrochim. Acta, 4, 362 (1961).
25. Yu. K. Delimarskii, K. M. Bojko, and G. W. Schilina, Electrochim. Acta, 6, 215 (1962).
26. T. N. Kaptsova and Yu. K. Delimarskii, Ukr. Khim. Zh., 29, 714 (1963).
27. R. Monnier and P. Tissot, Helv. Chim. Acta., 47, 2203 (1964).
28. A. Rius, F. Colom, and A. Artacho, Electrochim. Acta, 11, 1497 (1966).
29. R. G. Verdick and L. F. Yntema, J. Phys. Chem., 48, 268 (1944).

30. I. Seo, Japanese Patent 2258, April 5, 1958; CA 53, 11067e (1959).
31. P. Brouillet and I. Epelboin, Rev. mét., 51, 693 (1954).
32. H. A. Laitinen and C. H. Liu, J. Amer. Chem. Soc., 80, 1015 (1958).
33. G. Delarue, J. Electroanal. Chem., 1, 13 (1959).
34. M. Hansen and K. Anderko, Constitution of Binary Alloys, p.206, McGraw-Hill Book Co., Second Ed., New York (1958).
35. V. P. Mashovets and Yu. I. Aleksandrov, Zhur. Priklad. Khim., 43, 811 (1970).
36. K. E. Johnson and J. R. Mackenzie, Anal. Chem., 41, 1483 (1969).
37. H. A. Laitinen and H. C. Gaur, Anal. Chim. Acta, 18, 1 (1958).
38. T. Berzins and P. Delahay, J. Amer. Chem. Soc., 75, 4205 (1953).
39. O. J. Kleppa, J. Amer. Chem. Soc., 72, 3346 (1950).
40. O. J. Kleppa, J. Amer. Chem. Soc., 71, 3275 (1949).
41. R. I. Jaffee, E. M. Smith and B. W. Gonser, Trans. AIME, 161, 366 (1945).
42. C. W. Oatley, W. C. Nixon, and R. F. Pease, Advances in Electronics and Electron Physics, Vol. 21, pp.181-247, Academic Press, New York (1965).

43. W. Nixon, *Contemp. Phys.*, 10, 71 (1969).
44. A. C. Reimschuessel, *J. Chem. Educ.*, 49, A413 (1972).
45. H. A. Laitinen and J. W. Pankey, *J. Amer. Chem. Soc.*,
81, 1053 (1959).

A P P E N D I X IIntroduction

This section deals with some aspects of the electrochemistry of cobalt, manganese, and antimony in the fused LiCl-KCl eutectic at 450°C. The results of the experimental work carried out with these elements are reported in this separate section, as they are not a part of either of the integral units presented in Part I or Part II of this thesis. The information obtained in the study of cobalt and manganese define these two systems in the melt, but the results of the antimony study are only preliminary in nature.

Literature

The standard electrode potentials of the Mn(II)/Mn(0), Co(II)/Co(0), and Sb(III)/Sb(0) couples were determined in the fused LiCl-KCl eutectic by Laitinen and Liu (1), and were found to be -1.849 ± 0.008 V, -0.991 ± 0.003 V, and -0.635 ± 0.002 V, respectively at 450°C. Spectrophotometric study of Co(II) by Harrington and Sundheim (2), and Sundheim and Kukk (3), and of Mn(II) by Sundheim and Kukk (3) in the fused LiCl-KCl eutectic has shown that these species are tetrahedrally coordinated in the melt.

Delarue (4) and Colom and de la Cruz (5) have reported the solubility of Sb_2O_3 in the fused LiCl-KCl eutectic melt at temperatures above 500°C. Colom and de la Cruz (5)

stated that dissolution of Sb_2O_3 takes place in less than one hour at 600°C , and that solutions of Sb_2O_3 more concentrated than 0.03 mole fraction ($\sim 1\text{M}$) exist in the melt over the temperature range from 400°C to 600°C .

Experimental

The apparatus, chemicals, and technique employed in carrying out the electrochemical measurements have been described in Part I of this thesis. Cobalt was obtained in wire form (0.040" in diameter) from A. D. Mackay Inc., N.Y. The wire was cleaned with emery cloth, wound in the form of a spiral, degreased in carbon tetrachloride, and preanodized in the bulk melt before being placed into its isolation compartment.

Manganese metal was obtained in chip form from Alpha Inorganics, Beverly, Mass., and was 99.97% pure. A manganese chip was silver soldered to a copper wire which led out of the electrochemical cell. The manganese chip was cleaned in dilute hydrochloric acid, rinsed with distilled water, immersed in acetone, and air dried before being placed into the eutectic melt. Only part of the manganese chip was immersed into the melt to ensure that the melt did not come into contact with the solder or the copper wire.

Antimony was obtained in lump form (Alpha Inorganics, 99.9999% pure). The antimony was suspended into the melt

by a platinum wire because platinum and antimony do not alloy at 450°C (6). The antimony electrode was immersed into its isolation compartment after 18 hours of contact with the bulk melt. This precaution was taken to assure dissolution of any Sb_2O_3 that may have been present on the electrode surface. Barium oxide was prepared by thermal decomposition of BaCO_3 in vacuum, and served as a source of oxide ion in the antimony study. Antimony(III) oxide was obtained from Allied Chemical, N.Y., and was 99.0% pure. It was oven dried at 110°C prior to use.

R E S U L T S A N D D I S C U S S I O N

Manganese

The manganese chip did not react with the melt, and was anodized at a current density of approximately 10 mA/cm². Several data points were taken in the course of this anodization, and a plot of the cell potential as a function of the number of equivalents passed showed that manganese was being oxidized to Mn(II) at roughly the standard potential reported by Laitinen and Liu (1) for the Mn(II)/Mn(0) system. Attempts to further oxidize Mn(II) at a graphite electrode resulted in chlorine evolution. This shows that Mn(II) is the highest oxidation state of the element in the fused LiCl-KCl eutectic. Delarue (4) has reported that atmospheric contact with the LiCl-KCl eutectic melt containing Mn(II) results in the production of Mn₂O₃, which precipitates from solution.

Cobalt

The cobalt wire did not react with the melt, and was anodized at a current density of approximately 10 mA/cm² to give a blue solution of Co(II) at roughly the standard potential reported by Laitinen and Liu (1) for the Co(II)/Co(0) system. Delarue (4) employed voltammetry to show that anodization of Co(II) within the potential range of the melt was not possible. This result is supported;

the present attempt to oxidize Co(II) at a graphite electrode resulted in chlorine evolution. Thus, oxidation states of cobalt greater than Co(II) do not exist in the melt.

Antimony

Antimony does not react with the fused LiCl-KCl eutectic at 450°C. The antimony electrode was anodized to prepare a solution of Sb(III) for use in an attempt to determine the standard potential of the Sb(V)/Sb(III) redox couple. Twenty-five data points were collected in two separate experiments in order to calculate the standard potential of the Sb(III)/Sb(0) couple, and compare it with the value obtained by Laitinen and Liu (1). The current density employed in the oxidation of antimony was approximately 5 mA/cm². The concentration of Sb(III) ranged from 6.05×10^{-3} to 3.25×10^{-2} M. A plot of the number of equivalents passed as a function of the cell potential was linear and had a slope of 0.046 ± 0.002 V/log unit, in agreement with the theoretical value of 0.048 V/log unit for a three-electron process at 450°C. The standard potential of the Sb(III)/Sb(0) couple was calculated to be -0.624 ± 0.002 V, compared to the value of -0.635 ± 0.002 V obtained by Laitinen and Liu (1) for the same system.

Delarue (4) has reported that Sb(III) can be chemi-

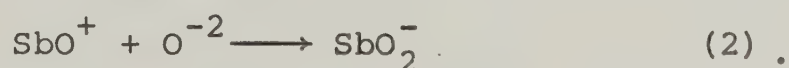
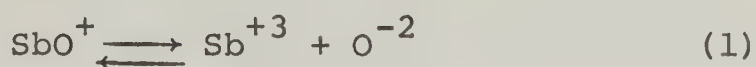
cally oxidized by Cu(II) to Sb(V), which volatilizes from the melt as $\text{SbCl}_5(\text{g})$. Since the standard potential of the Cu(II)/Cu(I) couple is +0.061 V (1), the standard potential of the Sb(V)/Sb(III) couple must then be less than this value. However, present attempts to oxidize Sb(III) to Sb(V) at a graphite anode at low current densities resulted in chlorine evolution, as was shown by the potential of the graphite anode. Since Delarue (4) did not purify his melt, it is possible that the presence of water in his system may account for the discrepancy, the oxidation observed being that of an oxygen-containing antimony species.

The electrochemistry of Sb(III) was found to be extremely sensitive to the presence of oxide. Barium oxide is soluble in the LiCl-KCl eutectic melt at 450°C. Addition of this compound to a solution of Sb(III) drastically decreased the potential of the cell (the cell potential decreased as much as 1.2 V from its initial value with increased addition of BaO), thereby showing that Sb(III) reacts quantitatively with oxide. Potentiometric data analysis showed that more than one oxy-complex of antimony was formed, depending upon the amount of BaO added to solution. The presence of more than one oxy-complex of antimony was confirmed by voltammetry. For example, a voltammetric scan of a solution prepared by the addition of BaO to Sb(III) such that the mole ratio of O^{-2} to Sb(III) was approximately 2:1 exhibited two reduction waves

whose half-wave potentials were -0.5 and -1.1 V.

Antimony(III) oxide was added to the LiCl-KCl eutectic at 450°C, in an amount much less than the saturation limit reported by Colum and de la Cruz (5), but did not dissolve even after having been in the melt for a period of four hours. Addition of BaO to the compartment into which the Sb_2O_3 was added resulted in the immediate dissolution of Sb_2O_3 . This is not surprising, since a reaction of the type $\text{Sb}_2\text{O}_3(\text{s}) + \text{O}^{-2} \longrightarrow \text{SbO}_2^-$ may have taken place. (Metantimonite, SbO_2^- , is a well-known species (7)). Delarue (4) and Colom and de la Cruz (5) did not completely eliminate water from their melts, and thus the presence of OH^- or O^{-2} in their systems would account for the rapid dissolution of Sb_2O_3 which they observed.

Attempts to synthesize SbOCl (to study the Sb/SbOCl system) were not successful. The procedures of Edstrand (8) and that reported by Brauer (9) were followed, but the compounds produced had physical properties that did not correspond to those ascribed to SbOCl . In view of the complex nature of the oxy-species of antimony in the melt, the Sb/SbOCl electrode would probably not be a simple system, since dissociation of SbO^+ (if SbOCl is soluble in the melt) may result in the formation of other oxy-complexes of Sb(III) :



Reaction (2) would occur if SbO_2^- is more stable than SbO^+ .

B I B L I O G R A P H Y

1. H. A. Laitinen and C. H. Liu, J. Amer. Chem. Soc., 80, 1015 (1958).
2. G. Harrington and B. R. Sundheim, Ann. N.Y. Acad. Sci., 79, 950 (1960).
3. B. Sundheim and M. Kukk, Disc. Far. Soc., 32, 49 (1961).
4. G. Delarue, J. Electroanal. Chem., 1, 285 (1959).
5. F. Colom and M. de la Cruz, Electrochim. Acta, 15, 749 (1970).
6. M. Hansen and K. Anderko, Constitution of Binary Alloys, Second Ed., p.1139, McGraw-Hill Book Co., New York, 1958.
7. J. W. Mellor, A Comprehensive Treaty on Inorganic and Theoretical Chemistry, Vol. IX, p.430, Longman, Greens, and Co., London, 1929.
8. M. Edstrand, Arkiv För Kemi, 6, 89 (1953).
9. G. Brauer (Ed.), Handbook of Preparative Inorganic Chemistry, Vol. 1, p.611, Academic Press, New York, 1963.

A P P E N D I X I I

P O T E N T I O M E T R I C D A T A

ANODIZATION OF Ga(0)

1. Reference Electrode

Volume of the reference compartment = 7.96 cm^3 .

Equivalents of Pt(II) generated = 1.200×10^{-4} .

Gallium Electrode

Volume of the gallium compartment = 6.95 cm^3 .

<u>Equivalents ($\times 10^4$)</u>	<u>Potential(V)</u>	<u>Equivalents ($\times 10^4$)</u>	<u>Potential(V)</u>
1.000	-1.126	5.400	-1.082
1.400	-1.120	7.600	-1.077
2.000	-1.108	10.151	-1.075
2.800	-1.101	14.295	-1.071
3.800	-1.088		

2. Reference Electrode

Volume of the reference compartment = 7.96 cm^3 .

Equivalents of Pt(II) generated = 1.200×10^{-4} .

Gallium Electrode

Volume of the gallium compartment = 7.15 cm^3 .

<u>Equivalents</u> <u>($\times 10^5$)</u>	<u>Potential(V)</u>	<u>Equivalents</u> <u>($\times 10^5$)</u>	<u>Potential(V)</u>
5.000	-1.169	38.000	-1.098
7.000	-1.163	54.000	-1.093
10.000	-1.150	76.000	-1.083
20.000	-1.117	100.000	-1.081
28.000	-1.109	130.220	-1.066

3. Reference Electrode

Volume of the reference compartment = 7.72 cm^3 .

Equivalents of Pt(II) generated = 1.200×10^{-4} .

Gallium Electrode

Volume of the gallium compartment = 7.05 cm^3 .

<u>Equivalents</u> <u>($\times 10^4$)</u>	<u>Potential(V)</u>	<u>Equivalents</u> <u>($\times 10^4$)</u>	<u>Potential(V)</u>
1.400	-1.100	5.562	-1.055
2.000	-1.091	7.600	-1.050
2.800	-1.082	10.600	-1.047
3.800	-1.067	15.000	-1.041

ANODIZATION OF In(0)1. Reference Electrode

Volume of the reference compartment = 2.75 cm^3 .

Equivalents of Pt(II) generated = 1.223×10^{-4} .

Indium Electrode

Volume of the indium compartment = 3.22 cm^3 .

<u>Equivalents</u> <u>($\times 10^5$)</u>	<u>Potential (V)</u>	<u>Equivalents</u> <u>($\times 10^5$)</u>	<u>Potential (V)</u>
5.000	-1.339	28.000	-1.236
7.000	-1.331	39.000	-1.211
10.000	-1.319	54.000	-1.192
14.000	-1.288	76.000	-1.173
20.038	-1.260		

2. Reference Electrode

Volume of the reference compartment = 5.33 cm^3 .

Equivalents of Pt(II) generated = 1.200×10^{-4} .

Indium Electrode

Volume of the indium compartment = 5.50 cm^3 .

Equivalents ($\times 10^5$)	Potential (V)	Equivalents ($\times 10^5$)	Potential (V)
5.000	-1.371	38.000	-1.281
7.000	-1.318	54.000	-1.258
10.000	-1.323	76.000	-1.236
14.000	-1.322	103.570	-1.204
20.000	-1.260	186.680	-1.153
28.000	-1.300		

3. Reference Electrode

Volume of the reference compartment = 5.33 cm^3 .

Equivalents of Pt(II) generated = 1.200×10^{-4} .

Indium Electrode

Volume of the indium compartment = 5.06 cm^3 .

Equivalents ($\times 10^4$)	Potential (V)	Equivalents ($\times 10^4$)	Potential (V)
1.000	-1.316	3.800	-1.236
1.400	-1.305	5.400	-1.209
2.000	-1.295	7.600	-1.185
2.800	-1.245	10.633	-1.181

4. Reference Electrode

Volume of the reference compartment = 7.72 cm^3 .

Equivalents of Pt(II) generated = 1.200×10^{-4} .

Indium Electrode

Volume of the indium compartment = 8.03 cm^3 .

Equivalents ($\times 10^4$)	Potential(V)	Equivalents ($\times 10^4$)	Potential(V)
1.400	-1.272	5.400	-1.194
2.000	-1.252	7.600	-1.174
2.800	-1.237	10.600	-1.153
3.800	-1.216		

ANODIZATION of In(I)1. Reference Electrode

Volume of the reference compartment = 2.75 cm^3 .

Equivalents of Pt(II) generated = 1.200×10^{-4} .

Indium Electrode

Equivalents of In(I) initially present = 7.600×10^{-4} .

Equivalents ($\times 10^5$)	Potential(V)	Equivalents ($\times 10^5$)	Potential(V)
1.000	-0.955	14.000	-0.889
3.000	-0.937	20.038	-0.874
5.000	-0.923	28.000	-0.857
7.000	-0.914	39.000	-0.834
10.000	-0.902		

2. Reference Electrode

Volume of the reference compartment = 5.33 cm^3 .

Equivalents of Pt(II) generated = 1.200×10^{-4} .

Indium Electrode

Equivalents of In(I) initially present = 1.0633×10^{-3} .

Equivalents ($\times 10^4$)	Potential(V)
5.515	-0.904
7.333	-0.885
10.634	-0.847
13.000	-0.809

3. Reference Electrode

Volume of the reference compartment = 7.72 cm^3 .

Equivalents of Pt(II) generated = 1.200×10^{-4} .

Indium Electrode

Equivalents of In(I) initially present = 1.060×10^{-3} .

Equivalents ($\times 10^4$)	Potential(V)	Equivalents ($\times 10^4$)	Potential(V)
1.000	-0.896	5.400	-0.820
1.400	-0.885	7.600	-0.803
2.000	-0.863	10.600	-0.785
2.800	-0.846	15.000	-0.757
3.800	-0.833		

ANODIZATION OF Tl(0)1. Reference Electrode

Volume of the reference compartment = 7.06 cm^3 .

Equivalents of Pt(II) generated = 1.200×10^{-4} .

Thallium Electrode

Volume of the thallium compartment = 6.72 cm^3 .

Equivalents ($\times 10^4$)	Potential(V)	Equivalents ($\times 10^4$)	Potential(V)
1.400	-1.551	2.800	-1.510
1.700	-1.540	3.300	-1.501
2.000	-1.529	3.800	-1.493
2.400	-1.520	4.600	-1.482

ANODIZATION OF Tl(I)1. Reference Electrode

Volume of the reference compartment = 6.81 cm^3 .

Equivalents of Pt(II) generated = 1.200×10^{-4} .

Thallium Electrode

Equivalents of Tl(I) initially present = 1.000×10^{-3} .

<u>Equivalents ($\times 10^5$)</u>	<u>Potential(V)</u>	<u>Equivalents ($\times 10^5$)</u>	<u>Potential(V)</u>
8.000	+0.202	40.000	+0.260
10.200	+0.210	44.500	+0.264
12.000	+0.216	50.000	+0.268
14.000	+0.221	57.000	+0.274
16.000	+0.226	62.000	+0.278
18.000	+0.230	67.000	+0.282
22.000	+0.237	72.000	+0.284
25.000	+0.242	76.000	+0.287
28.000	+0.246	80.000	+0.289
31.000	+0.250	84.000	+0.291
34.000	+0.254	90.000	+0.296

2. Reference Electrode

Volume of the reference compartment = 6.81 cm^3 .

Equivalents of Pt(II) generated = 1.200×10^{-4} .

Thallium Electrode

Equivalents of Tl(I) initially present = 1.000×10^{-3} .

Equivalents ($\times 10^5$)	Potential(V)	Equivalents ($\times 10^5$)	Potential(V)
7.000	+0.203	12.000	+0.220
8.000	+0.207	14.000	+0.225
9.000	+0.210	16.000	+0.230
10.200	+0.214	18.000	+0.234

ANODIZATION OF Ge(0)1. Reference Electrode

Volume of the reference compartment = 5.06 cm^3 .

Equivalents of Pt(II) generated = 1.201×10^{-4} .

Germanium Electrode

Volume of the germanium compartment = 5.87 cm^3 .

Equivalents ($\times 10^4$)	Potential(V)	Equivalents ($\times 10^4$)	Potential(V)
2.800	-0.764	7.600	-0.724
4.000	-0.748	10.800	-0.714
5.600	-0.735	14.200	-0.705

2. Reference Electrode

Volume of the reference compartment = 5.33 cm^3 .

Equivalents of Pt(II) generated = 1.200×10^{-4} .

Germanium Electrode

Volume of the germanium compartment = 6.41 cm^3 .

Equivalents ($\times 10^4$)	Potential(V)	Equivalents ($\times 10^4$)	Potential(V)
2.800	-0.783	7.600	-0.745
4.000	-0.766	10.800	-0.733
5.600	-0.754	14.200	-0.724

3. Reference Electrode

Volume of the reference compartment = 5.33 cm^3 .

Equivalents of Pt(II) generated = 1.200×10^{-4} .

Germanium Electrode

Volume of the germanium compartment = 6.04 cm^3 .

Equivalents ($\times 10^4$)	Potential(V)	Equivalents ($\times 10^4$)	Potential(V)
2.000	-0.808	7.600	-0.757
2.800	-0.793	10.800	-0.746
4.000	-0.778	14.200	-0.736
5.600	-0.776		

4. Reference Electrode

Volume of the reference compartment = 2.26 cm^3 .

Equivalents of Pt(II) generated = 1.500×10^{-4} .

Germanium Electrode

Volume of the germanium compartment = 1.82 cm^3 .

Equivalents ($\times 10^5$)	Potential(V)	Equivalents ($\times 10^5$)	Potential(V)
0.500	-0.895	8.000	-0.808
1.000	-0.877	16.000	-0.787
2.000	-0.853	32.000	-0.769
4.000	-0.830	40.000	-0.762

ANODIZATION OF Ge(II)1. Reference Electrode

Volume of the reference compartment = 5.33 cm^3 .

Equivalents of Pt(II) generated = 1.200×10^{-4} .

Germanium Electrode

Volume of the germanium compartment = 6.41 cm^3 .

Equivalents of Ge(II) initially present = 1.420×10^{-3} .

Equivalents ($\times 10^4$)	Potential(V)
2.000	-0.448
2.800	-0.446
4.000	-0.441
5.600	-0.439

2. Reference Electrode

Volume of the reference compartment = 5.33 cm^3 .

Equivalents of Pt(II) generated = 1.200×10^{-4} .

Germanium Electrode

Volume of the germanium compartment = 6.04 cm^3 .

Equivalents of Ge(II) initially present = 1.420×10^{-3} .

Equivalents

<u>($\times 10^4$)</u>	<u>Potential(V)</u>
2.000	-0.450
2.800	-0.449
4.000	-0.444
5.600	-0.437

ANODIZATION OF Sn(0)1. Reference Electrode

Volume of the reference compartment = 6.39 cm^3 .

Equivalents of Pt(II) generated = 1.201×10^{-4} .

Tin Electrode

Volume of the tin compartment = 5.94 cm^3 .

Equivalents ($\times 10^4$)	Potential (V)	Equivalents ($\times 10^4$)	Potential (V)
2.000	-1.053	7.600	-0.997
2.800	-1.042	10.000	-0.987
3.800	-1.028	13.000	-0.977
5.400	-1.011		

ANODIZATION OF Sn(II)

1. Reference Electrode

Volume of the reference compartment = 7.33 cm^3 .

Equivalents of Pt(II) generated = 1.200×10^{-4} .

Tin Electrode

Equivalents of Sn(II) initially present = 2.200×10^{-3} .

Equivalents ($\times 10^4$)	Potential (V)	Equivalents ($\times 10^4$)	Potential (V)
2.800	-0.214	4.000	-0.199
3.400	-0.208	4.800	-0.191

2. Reference Electrode

Volume of the reference compartment = 7.79 cm^3 .

Equivalents of Pt(II) generated = 1.200×10^{-4} .

Tin Electrode

Equivalents of Sn(II) initially present = 2.200×10^{-3} .

Equivalents ($\times 10^4$)	Potential(V)	Equivalents ($\times 10^4$)	Potential(V)
2.852	-0.213	4.000	-0.204
3.400	-0.209	4.800	-0.198

3. Reference Electrode

Volume of the reference compartment = 7.54 cm^3 .

Equivalents of Pt(II) generated = 1.200×10^{-4} .

Tin Electrode

Equivalents of Sn(II) initially present = 2.200×10^{-3} .

Equivalents ($\times 10^4$)	Potential(V)	Equivalents ($\times 10^4$)	Potential(V)
2.800	-0.214	3.700	-0.205
3.100	-0.211	4.000	-0.202
3.400	-0.208	4.250	-0.201

ANODIZATION OF Pb(0)1. Reference Electrode

Volume of the reference compartment = 7.64 cm^3 .

Equivalents of Pt(II) generated = 1.200×10^{-4} .

Lead Electrode

Volume of the lead compartment = 6.99 cm^3 .

Equivalents ($\times 10^4$)	Potential(V)	Equivalents ($\times 10^4$)	Potential(V)
2.800	-1.054	9.200	-1.021
4.000	-1.045	10.800	-1.017
4.900	-1.039	13.000	-1.010
5.600	-1.038	15.200	-1.006
6.636	-1.032	17.600	-1.002
7.600	-1.026		

ANODIZATION OF Sb(0)1. Reference Electrode

Volume of the reference compartment = 6.47 cm^3 .

Equivalents of Pt(II) generated = 1.200×10^{-4} .

Antimony Electrode

Volume of the antimony compartment = 7.71 cm^3 .

Equivalents ($\times 10^4$)	Potential(V)	Equivalents ($\times 10^4$)	Potential(V)
1.400	-0.584	3.510	-0.564
1.700	-0.578	4.000	-0.562
2.000	-0.574	4.600	-0.558
2.250	-0.572	5.400	-0.557
2.500	-0.569	6.200	-0.554
2.750	-0.570	7.000	-0.552
3.000	-0.568		

2. Reference Electrode

Volume of the reference compartment = 6.47 cm^3 .

Equivalents of Pt(II) generated = 1.200×10^{-4} .

Antimony Electrode

Volume of the antimony compartment = 7.17 cm^3 .

Equivalents ($\times 10^4$)	Potential(V)	Equivalents ($\times 10^4$)	Potential(V)
1.400	-0.582	3.500	-0.565
1.700	-0.579	4.000	-0.563
2.000	-0.577	4.600	-0.561
2.250	-0.575	5.400	-0.557
2.500	-0.571	6.200	-0.554
3.000	-0.566	7.000	-0.552

SAMPLE CALCULATION OF THE STANDARD POTENTIAL

Consider the first entry on page 138 (2.000×10^{-4} equivalents, -1.053 V). This corresponds to the first data point obtained in the anodization of Sn(0).

1. Reference Electrode

For $\text{Pt}(0) \longrightarrow \text{Pt}(\text{II}) + 2e^-$, $E = E^\circ + \frac{0.1434}{2} \log [\text{Pt}(\text{II})]$.

Thus, $E = 0.000 + \frac{0.1434}{2} \log \left(\frac{1.201 \times 10^{-4}}{2 \times 6.39 \times 10^{-3}} \right)$, and

$E = -0.148 \text{ V}$.

2. Tin Electrode

$E_{\text{cell}} = E_+ - E_-$, where E_{cell} = equilibrium cell potential.

Since the tin electrode was negative with respect to the platinum electrode, E_+ = reference electrode potential, and E_- = indicating (tin) electrode potential. Thus, $1.053 = -0.148 - E_-$, and $E_- = -1.201$ V.

For $\text{Sn}(0) \longrightarrow \text{Sn}(\text{II}) + 2e^-$,

$$E_- = E^\circ + \frac{0.1434}{2} \log [\text{Sn}(\text{II})].$$

$$\text{Thus, } -1.201 = E^\circ + \frac{0.1434}{2} \log \left(\frac{2.000 \times 10^{-4}}{2 \times 5.93 \times 10^{-3}} \right), \text{ and}$$

$$E^\circ = -1.073 \text{ V.}$$

Once the individual standard potentials were obtained in this manner, the mean value and standard deviation of the series of the standard potentials were calculated. The theoretical value of the prelogarithmic term in the Nernst equation was employed in all standard potential calculations.

B30056